Available online at www.sciencedirect.com
SCIENCE DIRECT
ELSEVIER
Icarus 176 (2005) 351–381
ICARUS
www.elsevier.com/locate/icarus

The rayed crater Zunil and interpretations of small impact craters on Mars

Alfred S. McEwen [a,*], Brandon S. Preblich [a], Elizabeth P. Turtle [a], Natalia A. Artemieva [b], Matthew P. Golombek [c], Michelle Hurst [d], Randolph L. Kirk [e], Devon M. Burr [e], Philip R. Christensen [f]

[a] *Department of Planetary Sciences, Lunar and Planetary Lab, University of Arizona, Tucson, AZ 85721, USA*
[b] *Institute for Dynamics of Geospheres, Russian Academy of Sciences, Moscow, Russia*
[c] *Jet Propulsion Laboratory, California Institute of Technology, Pasadena, CA 91109, USA*
[d] *Department of Geology, Brigham Young University, Provo, UT 84602, USA*
[e] *U.S. Geological Survey, Astrogeology Team, 2255 N. Gemini Drive, Flagstaff, AZ 86001, USA*
[f] *Department of Geological Sciences, Arizona State University, Tempe, AZ 85287, USA*

Received 9 April 2004; revised 11 February 2005

Available online 15 April 2005

Abstract

A 10-km diameter crater named Zunil in the Cerberus Plains of Mars created $\sim 10^7$ secondary craters 10 to 200 m in diameter. Many of these secondary craters are concentrated in radial streaks that extend up to 1600 km from the primary crater, identical to lunar rays. Most of the larger Zunil secondaries are distinctive in both visible and thermal infrared imaging. MOC images of the secondary craters show sharp rims and bright ejecta and rays, but the craters are shallow and often noncircular, as expected for relatively low-velocity impacts. About 80% of the impact craters superimposed over the youngest surfaces in the Cerberus Plains, such as Athabasca Valles, have the distinctive characteristics of Zunil secondaries. We have not identified any other large ($\geqslant$10 km diameter) impact crater on Mars with such distinctive rays of young secondary craters, so the age of the crater may be less than a few Ma. Zunil formed in the apparently youngest (least cratered) large-scale lava plains on Mars, and may be an excellent example of how spallation of a competent surface layer can produce high-velocity ejecta (Melosh, 1984, Impact ejection, spallation, and the origin of meteorites, Icarus 59, 234–260). It could be the source crater for some of the basaltic shergottites, consistent with their crystallization and ejection ages, composition, and the fact that Zunil produced abundant high-velocity ejecta fragments. A 3D hydrodynamic simulation of the impact event produced 10^{10} rock fragments $\geqslant$10 cm diameter, leading to up to 10^9 secondary craters $\geqslant$10 m diameter. Nearly all of the simulated secondary craters larger than 50 m are within 800 km of the impact site but the more abundant smaller (10–50 m) craters extend out to 3500 km. If Zunil is representative of large impact events on Mars, then secondaries should be more abundant than primaries at diameters a factor of $\sim$1000 smaller than that of the largest primary crater that contributed secondaries. As a result, most small craters on Mars could be secondaries. Depth/diameter ratios of 1300 small craters (10–500 m diameter) in Isidis Planitia and Gusev crater have a mean value of 0.08; the freshest of these craters give a ratio of 0.11, identical to that of fresh secondary craters on the Moon (Pike and Wilhelms, 1978, Secondary-impact craters on the Moon: topographic form and geologic process, Lunar Planet. Sci. IX, 907–909) and significantly less than the value of $\sim$0.2 or more expected for fresh primary craters of this size range. Several observations suggest that the production functions of Hartmann and Neukum (2001, Cratering chronology and the evolution of Mars, Space Sci. Rev. 96, 165–194) predict too many primary craters smaller than a few hundred meters in diameter. Fewer small, high-velocity impacts may explain why there appears to be little impact regolith over Amazonian terrains. Martian terrains dated by small craters could be older than reported in recent publications.

* Corresponding author. Fax: +1 520 621 9628.
E-mail address: mcewen@pirl.lpl.arizona.edu (A.S. McEwen).

0019-1035/$ – see front matter
doi:10.1016/j.icarus.2005.02.009

Keywords: Mars; Cratering; Regoliths; Moon; Impact processes

1. Introduction

Are small (less than ~1 km diameter) craters on Mars and the Moon dominated by primary impacts, by secondary impacts of much larger primary craters, or are both primaries and secondaries significant? This question is critical to age constraints for young terrains and for older terrains covering small areas, where only small craters are superimposed on the unit. Many craters are obviously secondaries, closely associated with the primary crater and with distinctive morphologies such as shallow, irregular shapes and occurrence in chains and clusters, sometimes with distinctive herringbone patterns (e.g., Shoemaker, 1962; Oberbeck and Morrison, 1973). However, there has been a longstanding controversy about the relative abundances of small primaries versus distant secondaries on the Moon. Distant secondaries produced by high-velocity ejecta fragments are more circular and isolated than the obvious secondaries near the source crater, and are therefore difficult to distinguish from degraded (shallow) primaries. Shoemaker (1965) hypothesized that there may be enormous numbers of these distant or background secondaries.

McEwen et al. (2003) reported the discovery of rays of secondary craters extending more than 800 km from the primary, a 10.1-km diameter crater in the young volcanic plains of Cerberus (SE Elysium Planitia) (Fig. 1). This was the first discovery of a large rayed crater on Mars, similar to rayed craters like Tycho on the Moon. The IAU has approved the name "Zunil" for this crater, after a village in the western Guatemalan highlands known for its hot springs. Zunil provides a well-preserved example of a primary crater with enormous numbers of distant secondary craters. In this paper we review relevant past studies (Section 1), describe the observations of Zunil and associated secondary craters (Section 2), simulate the production of secondaries by Zunil (Section 3), describe evidence that most martian craters smaller than a few hundred meters diameter are secondaries (Section 4), and offer further discussion and interpretations (Section 5).

1.1. Relevance to recent geologic activity and climate change on Mars

Some of the most significant results from Mars Global Surveyor (MGS) have come from images of terrains and features that are nearly devoid of small (10–100 m diameter) impact craters (Malin and Edgett, 2001). These terrains and features include high-latitude gullies and aprons (Malin and Edgett, 2000a; Reiss et al., 2004), polygonal terrain (Siebert and Kargel, 2001), glaciers (Kargel, 2004; Neukum et al., 2004), lava flows and rootless cones (Keszthelyi et al., 2000; Lanagan et al., 2001), channels emanating from Cerberus Fossae (Burr et al., 2002b), fine layered deposits in polar and equatorial regions (Malin and Edgett, 2000b, 2001) including layered deposits in Meridiani Planum near where the Mars Exploration Rover (MER) Opportunity landed (Golombek et al., 2003; Squyres et al., 2004), "swiss cheese" terrain of the South Polar residual cap (Thomas et al., 2000; Malin et al., 2001), debris flows and lineated valley fill of the fretted terrain (Carr, 2001; Pierce and Crown, 2002), mid-latitude debris mantles (Mustard et al., 2001; Head et al., 2003), and deposits from larger impact craters (Mouginis-Mark et al., 2003). The paucity of small craters has generally been interpreted in one of two general ways: (1) as evidence for recent geologic activity such as volcanism, aqueous processes, and glacial and periglacial processes; or (2) as evidence for recent or ongoing eolian processes. These interpretations often imply that Mars has been internally active in very recent times, including magmatic and hydrothermal activity, and/or that there have been recent climate changes. The inferred youth of some of these features increases the likelihood of liquid water near the surface today or in the recent past, and provides high-priority targets for the future exploration of Mars. Potentially ancient layered deposits (many of which are free of small craters, so they appear to be actively eroding or to have been recently exposed) are also high-priority targets, as they provide access to deposits related to ancient aqueous processes (Malin and Edgett, 2000b, 2003).

However, uncertainty exists as to the absolute ages of the deposits or timing of the modification processes, which are key to understanding the physical processes and implications for climate change, and to planning future exploration. Is it possible for crater-free terrains with primary meter-scale morphologies to be older than a few Ma? If the gullies were typically only thousands of years old (Malin and Edgett, 2000a), then there could be active springs or snowmelt (Christensen, 2003) today, and NASA might justify an aggressive search for extant life near the surface. If the gullies were typically 10^6 to 10^8 yrs old, then the probability of finding significant amounts of liquid water at or very near the surface today would be much lower. If some fine-layered deposits were of Noachian age (Malin and Edgett, 2000b) then they might be more likely to record the environment of long-lived lakes than if they were Hesperian or Amazonian. Is it possible for fine-layered deposits to erode rapidly enough to remove small craters and yet persist for billions of years?

Hartmann and Neukum (Hartmann, 1999; Neukum et al., 2001; Hartmann and Neukum, 2001) have published model production functions for craters on Mars. We will use the abbreviations HPF and NPF for the production functions of Hartmann and of Neukum, respectively, referenced to the modifications of Ivanov (2001). The two functions are nearly identical except at rim-to-rim crater diameters (D) less than 60 m or from 2 to 10 km, where they differ by factors of 2 to 5. Both of these models are based on the assump-

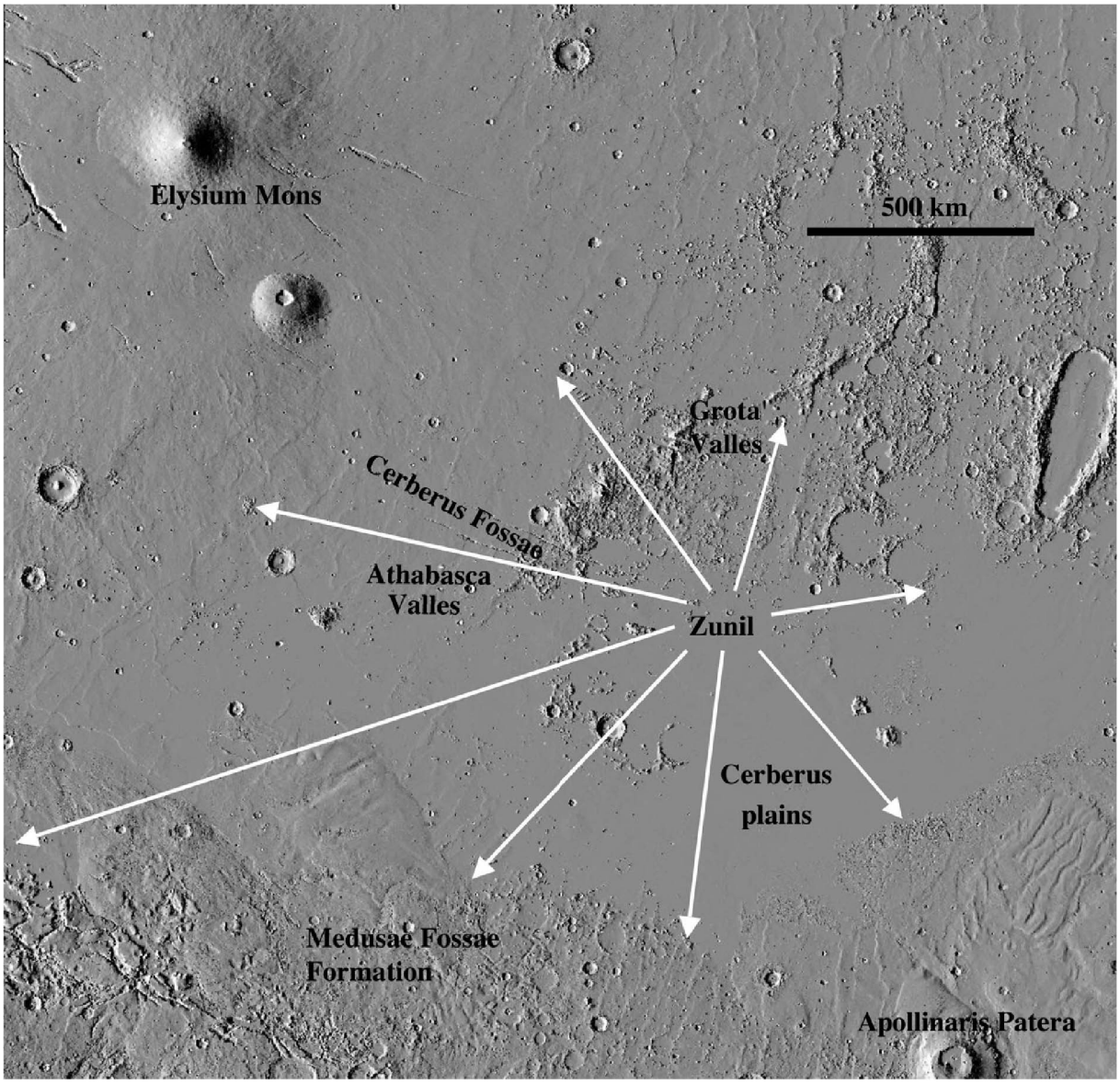

Fig. 1. MOLA shaded relief map of SE Elysium Planitia showing location of Zunil, its rays, and other features mentioned in the text. The region shown here extends from latitude 10° S to 30° N and longitude 140° E to 180° E.

tions that (1) objects striking Mars over time have the same size-frequency distribution as objects that cratered the Moon (Ivanov et al., 2002; see Strom et al., 1992 for a different interpretation); and (2) small craters on the Moon and Mars are dominated by primaries. Recent studies (e.g., Hartmann and Berman, 2000; Lanagan et al., 2001; Burr et al., 2002a; Berman and Hartmann, 2002; Mangold, 2003; Werner et al., 2003; Marquez et al., 2004; Quantin et al., 2004; Reiss et al., 2004; Neukum et al., 2004) have compared crater counts to the HPF or NPF, concluding that some lava flows, flood channels, landslides, and lobate debris aprons have very young ages, less than 10 Ma. Furthermore, the near-absence of impact craters superimposed on some terrains at high latitudes suggests ages of less than a few Ma for small areas or less than ∼0.2 Ma for large areas (Mustard et al., 2001; Schaller et al., 2003). These interpretations have garnered much attention because they suggest that fluvial and volcanic activity and climate change occurred in the very recent geologic past (e.g., Baker, 2001), perhaps correlated with the most recent cycle of high obliquity (Head et al., 2003). However, age constraints based on small craters must be reconsidered if secondary craters dominate the population.

1.2. A 40-year old lunar controversy: primaries vs secondaries

The size-frequency distribution (SFD) of craters over limited size ranges is commonly described by a power law of the form:

$$N(\geqslant D) = kD^{-b},$$

where N is the cumulative number of craters, D is crater diameter, k is a constant depending on crater density, and b is the power-law exponent or "slope." The SFD can also be presented as the differential number of craters (add 1 to the value of b to compare with the cumulative SFD), or in the logarithmic–differential format of Hartmann (same value of b as cumulative distribution except near changes of slope). In this paper we refer to b values appropriate for the cumulative or Hartmann plots. Primary craters on the Moon and Mars with diameters from about 1 to 100 km have $b \sim 2$ (Hartmann et al., 1981; Barlow, 1988; Strom et al., 1992; Hartmann, 1999), whereas well-resolved secondary craters produced by a single primary crater have a "steeper" SFD with $b \sim 3.5$ to 4 (Shoemaker, 1965; Wilhelms et al., 1978). The SFDs of the lunar maria and other plains, excluding obvious secondaries, show a steeper slope for craters smaller than ~1 km. Shoemaker (1965) presented a hypothetical model in which ~1 km is the crossover point between two distributions: primaries (with $b = 2$ at all sizes) dominate for craters larger than ~1 km and secondaries (with $b \sim 4$) dominate at smaller sizes. Shoemaker measured the SFD of secondary craters from the Sedan nuclear explosion crater in Nevada and several lunar craters. He noted that the crossover diameter should vary as a function of proximity to crater rays. Away from known lunar crater rays, Shoemaker estimated that distant secondaries dominate at crater diameters smaller than ~200 m, and he preferred a model of the primary production function that steepened to $b \sim 3$ at diameters less than ~1 km. Shoemaker's favored model is difficult to test on the Moon because the lunar maria reach a steady-state SFD (Shoemaker, 1965) or "saturation equilibrium" (Hartmann and Gaskell, 1997) at sizes smaller than ~250 m, and few craters larger than 100 m are present on young surfaces (not in saturation equilibrium) produced by large Copernican craters (Neukum and Koenig, 1976; McEwen et al., 1993).

Shoemaker's interpretation that secondaries dominate the cratering statistics below some crossover diameter was confirmed by other workers (e.g., Wilhelms et al., 1978 for basin secondaries) and applied to Mars (Soderblom et al., 1974), whereas others believed that small circular craters without herringbone patterns are chiefly primary (e.g., Neukum et al., 1975, 2001). Most subsequent workers have interpreted this controversy as whether or not the steeper slope at D less than ~1 km makes this the crossover diameter (where the number of secondaries exceeds the number of primaries), although that was not exactly the model favored by Shoemaker (1965). Neukum and Ivanov (1994) presented a critique of the secondary cratering model for Mars of Soderblom et al. (1974), showing that the crossover diameter must vary with the size of the largest contributing primary craters, i.e. it must vary with terrain age. They showed that a steeper SFD slope on the Moon (using the Soderblom et al. model) should occur at slightly larger than 10 km for ~4 Ga terrains (affected by late heavy bombardment) and at slightly less than 3 km for 3.2 Ga terrains (i.e., typical lunar maria). They wrote (p. 376) "But this is not observed. This fact is a strong argument against a secondary crater distribution in the range $D \leqslant 10$ km, and advocates clearly for the interpretation that we are dealing with a primary crater distribution over the whole range." However, the study of basin secondaries (i.e. ~3.9 Ga terrains) by Wilhelms et al. (1978) concluded that basin secondaries outnumber primaries at sizes smaller than 20 km. This result plus a crossover diameter at ~1 km or less on the maria is in accord with a shift in crossover diameter with terrain age.

The observation of a relatively steep SFD (b from 3.1 to 3.7) for small craters (~0.2 to 1 km) on the asteroid Gaspra, where secondaries are thought to be absent due to the very low escape velocity, has been considered strong evidence for a steep primary SFD for craters smaller than 1 km (Neukum and Ivanov, 1994; Chapman et al., 1996; Neukum et al., 2001). However, the *Galileo* observations of Gaspra did not provide reliable information on the SFD of craters smaller than ~200 m, and Gaspra may have a unique cratering history that cannot be used to calibrate the production function on the Moon or Mars.

There is growing recognition of the importance of the Yarkovsky effect (a weak but constant force due to thermal reemission of sunlight by rotating asteroids) and YORP (Yarkovsky–O'Keefe–Radzievskii–Paddack effect of thermal reemission on spin rates of irregular bodies). These effects largely control the orbital evolution and SFD of Earth-crossing asteroids (Morbidelli et al., 2002), such that near-Earth asteroids (NEAs) larger than 1 km (producing craters larger than 10 km) should have a SFD only slightly steeper than that in the main belt (Morbidelli and Vokrouhlicky, 2003). Modeling of the effects of thermal reemission and other processes on the SFD of NEAs smaller than 1 km has recently been completed (Bottke et al., 2005; O'Brian and Greenberg, submitted), and both studies conclude that the SFD of small asteroids both in the main belt and NEAs are not expected to steepen significantly at small sizes.

Useful evidence for the SFD of NEAs comes from direct observations, in spite of considerable incompleteness and observational bias (Jedicke et al., 2002). Observed bodies as small as 3 m diameter (Rabinowitz et al., 2000; Brown et al., 2002) have been reported to agree with the NPF, depending on choice of crater scaling models (Werner et al., 2002; Ivanov et al., 2002). Small NEAs probably originate as impact ejecta from asteroids, so it seems reasonable to find a similarly steep SFD as for ejecta from cratering on the Moon or Mars (Hartmann, 1969). However, reanalysis of these and other data by Bottke et al. (2005) shows that the observed NEA SFD probably does not explain the steep SFD of craters smaller than 1 km diameter on the Moon.

Some workers seem convinced that small craters of all sizes on the terrestrial planets are dominated by primaries; in recent review papers secondaries are either dismissed as unimportant (Neukum and Ivanov, 1994) or not mentioned (Hartmann and Neukum, 2001; Neukum et al., 2001; Ivanov et al., 2002). Hartmann (1999) took an intermediate

stance, arguing that the production function at $D < 1$ km may show more variation than the production function for larger craters due to variations in local secondary populations. However, there has been no convincing refutation of Shoemaker's (1965) measurements of the abundances of secondary craters and arguments for the significance of background secondaries.

1.3. Expected small-crater distributions on Mars

Should we expect distant secondary craters to be more or less common on Mars than on the Moon? Barlow (2003) compared the SFDs of obvious secondaries around six lunar and martian craters of comparable impact energies, and found fewer secondaries in the martian examples. However, these were obvious secondaries near the primary craters, which are excluded from crater counts for age determination. The key issue for age determination is the abundance of distant secondaries, which are not easily distinguished from primaries. Distant secondaries should constitute a greater fraction of small craters on Mars than on the Moon for several reasons:

(1) Primary impact velocities are lower on Mars (because it is further from the Sun) and secondary impact velocities can be higher on Mars (up to the 5 km/s escape velocity, vs 2.4 km/s escape velocity for the Moon). Hence, primary craters for a given projectile diameter will usually be smaller on Mars than on the Moon whereas distant secondaries will usually be larger on Mars.
(2) Mars has significant surface areas with little regolith, where even small impacts produce abundant high-velocity spalls (Melosh, 1984; Head et al., 2002).
(3) The atmosphere of Mars must reduce the density of small primary craters and flatten the SFD below some diameter limit (Melosh, 1989; Vasavada et al., 1993; Chappelow and Sharpton, 2003). Since breakup is proportional to velocity squared, the atmosphere should have less of an effect on the lower-velocity blocks larger than 10 cm diameter that produce secondary craters, even though they may pass though the atmosphere twice. [Ejecta fragments smaller than 10 cm will be significantly decelerated by Mars' current atmosphere on their way up (Artemieva and Ivanov, 2004).]

1.4. Secondary revival

The discoveries on Earth of meteorites from the Moon [predicted by Shoemaker (1965)] and Mars [reviewed by Nyquist et al. (2001)] should have made it obvious that distant secondary craters must be significant. Head et al. (2002) estimated that the probability that a rock ejected from Mars will land on Earth and be discovered is 10^{-6} to 10^{-7}. Thus, an impact event that delivered a discovered meteorite to Earth must have ejected at least 10^6 rocks larger than 3 cm in diameter at greater than Mars escape velocity (5 km/s). The hydrocode modeling of Head et al. (2002) indicates that the vertical impact of a 150-m projectile (producing a 3-km diameter crater) into basaltic plains with negligible regolith will eject $>10^7$ fragments larger than 3 cm (ignoring atmospheric deceleration). This is a small fraction of the high-velocity ejecta; most fragments must fall back onto Mars. Melosh (1984) and Vickery (1987) demonstrated a strong negative correlation between fragment size and ejection velocity, so most of the larger fragments make secondary craters rather than escaping Mars. In an oblique impact the amount of high-velocity ejecta increases by an order of magnitude (Artemieva and Ivanov, 2004). Such high-velocity fragments can land over widespread regions on Mars and might not be concentrated in identifiable rays.

Bierhaus et al. (2001) studied secondary craters produced by the 25-km diameter crater Pwyll on Europa, which has bright rays extending for over 1000 km. Their results revealed a steep SFD ($b \sim 3.2$), which suggests that Pwyll produced $\sim 10^5$ secondary craters larger than 50 m diameter, assuming the largest secondary crater had a diameter of 1.25 km (5% of primary; see Schultz and Singer, 1980; Melosh, 1989). Bierhaus et al. counted a total of over 29,500 craters on 95 images with resolutions better than 100 m/pixel (global sampling of 0.01% of Europa), and argued that the majority of small craters on Europa are strongly clustered and could be secondaries. The sparse primary cratering of Europa, due to its young surface and a relative paucity of small cometary bodies (Zahnle et al., 2003), makes the surface a "clean slate" for the study of secondary crater characteristics. Bierhaus et al. (2001) argued that their Europa results have implications for the Moon, Mars, and Mercury by reconfirming that huge numbers of secondary craters are possible.

2. The rayed crater Zunil

2.1. Discovery of the rayed crater

The many small (10–200 m) bright-rayed craters in the Cerberus region (Fig. 2) had been puzzling (e.g., Grier and Hartmann, 2000). They appear very fresh and well-preserved, with bright ejecta and fine rays extending up to distances of ~10 crater diameters. They are strongly clustered both locally and globally (most are in the Cerberus region). The crater rims are generally circular, but those imaged at the highest resolution appear more angular and unusually shallow (compared with fresh primary craters). Some of them consist of very tight clusters of overlapping craters (Fig. 2c). They range in size from the limits of MOC resolution (~10 m diameter) up to ~200 m. It is difficult to map out the distribution of these craters from the sparse coverage by narrow-angle MOC images.

Infrared (IR) images from THEMIS (thermal emission imaging system) have revealed exquisite details of well-preserved impact craters (Christensen et al., 2003). There are

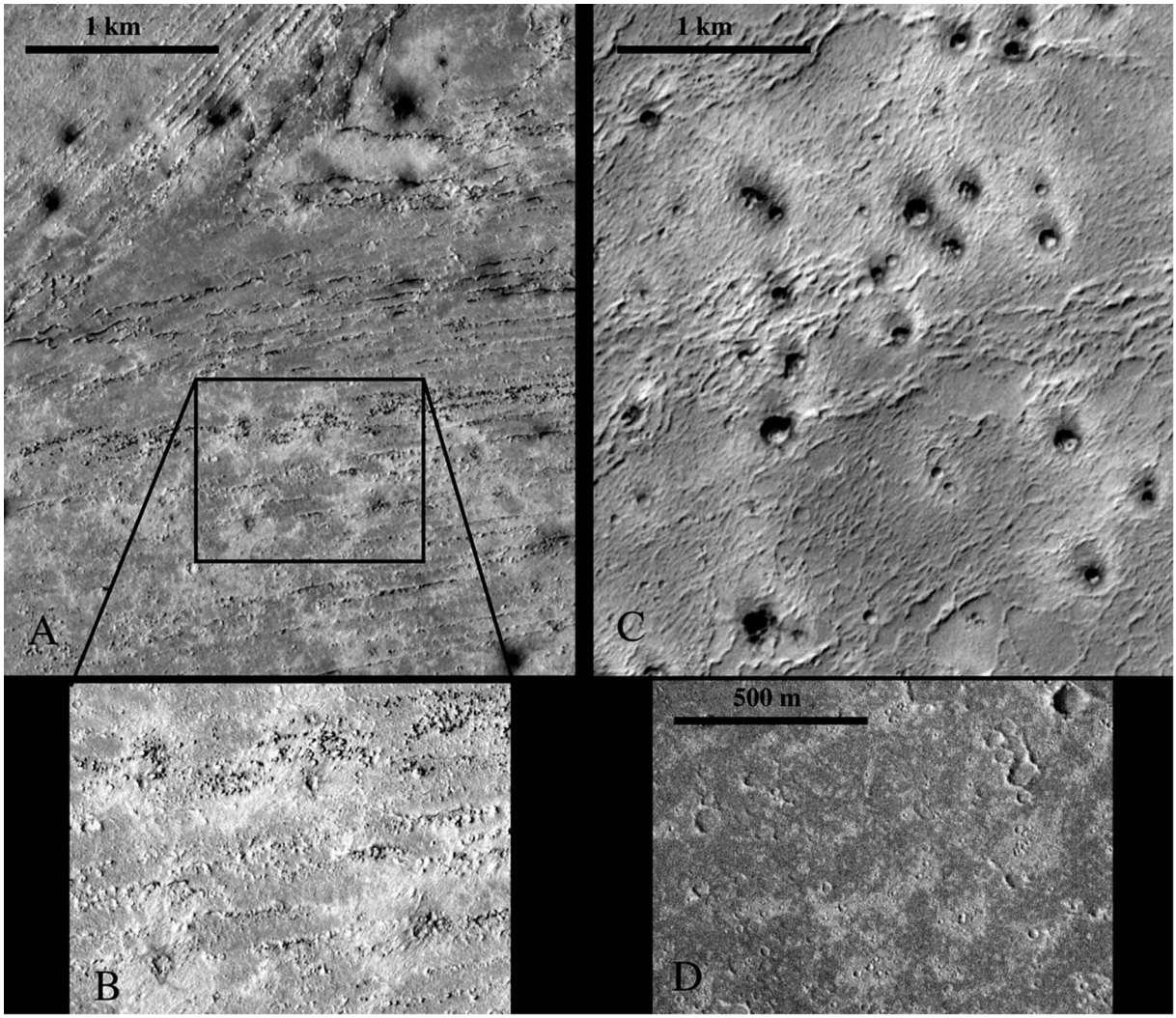

Fig. 2. MOC images showing secondary craters from Zunil. (A) shows part of M02-00581 at 5.9 m/pixel; image is 3 km wide. (B) shows part of the same region as in the bottom of (A) at 1.48 m/pixel from image E04-02119; image is ∼1 km wide. Note the nearly square rim of the crater near bottom left, which appears circular in (A). (C) shows large Zunil secondaries (up to 150 m diameter) in a portion of M21-00420 at 5.9 m/pixel; image is 3 km wide. (D) shows tight clusters of craters in part of M16-00228 at 1.47 m/pixel; image is ∼1.1 km wide. Probably only the small craters with bright ejecta in (D) are from Zunil, superimposed on a previously-cratered plain. North is ∼7 degrees to the right of up on these images and those in Figs. 3, 4, 6, 7, 8, 18, and 19.

strong variations in thermal inertia (TI) and albedo, apparent from early morning and late afternoon temperatures and visible images. The fresh craters in the Elysium region typically have 3 facies: (1) very high-TI, low-albedo crater rims and interiors; (2) moderate- to high-TI and moderate-albedo inner ejecta, and (3) low-TI and high-albedo outer ejecta and fine rays (Fig. 3). The high-TI, low-albedo material is rocky, as expected from lunar and terrestrial craters. The low-TI ejecta facies may be unique to Mars. The TI and albedo of this material are similar to those of the ubiquitous martian dust, but the fine ejecta may be lightly sintered or cemented to allow the fine structure of the ejecta to be preserved for more than a few years in the active eolian environment. Also, the bright ejecta may be the source for nearby bright dunes. These dunes have very low TIs similar to ejecta facies (3), consistent with micron-sized dust, but must be sintered or agglomerated into larger particles in order to saltate and form dunes (Greeley and Iverson, 1985). A possible origin for the outer facies is atmospheric winnowing of fine particles from the expanding ejecta curtain, producing a turbulent cloud that collapses to produce radially directed density currents. This idea was proposed by Schultz and Gault (1979) to explain large fluidized ejecta blankets, but might apply to the dusty outer ejecta facies described here. Impact mobilization of dust in the martian atmosphere has been modeled by Nemtchinov et al. (2002), who found that a 2-m diameter meteoroid impacting at 20 km/s raises a dust cloud to an altitude of about 2 km. Zunil's secondary craters were created by much lower-velocity impacts, <5 km/s depending on range and ejection angle, so perhaps they raised dust clouds a few hundred meters high. This fine outer facies shows various degrees of wind erosion (Fig. 4), so it is likely to be present only around very young craters, and probably disappears more rapidly from smaller craters.

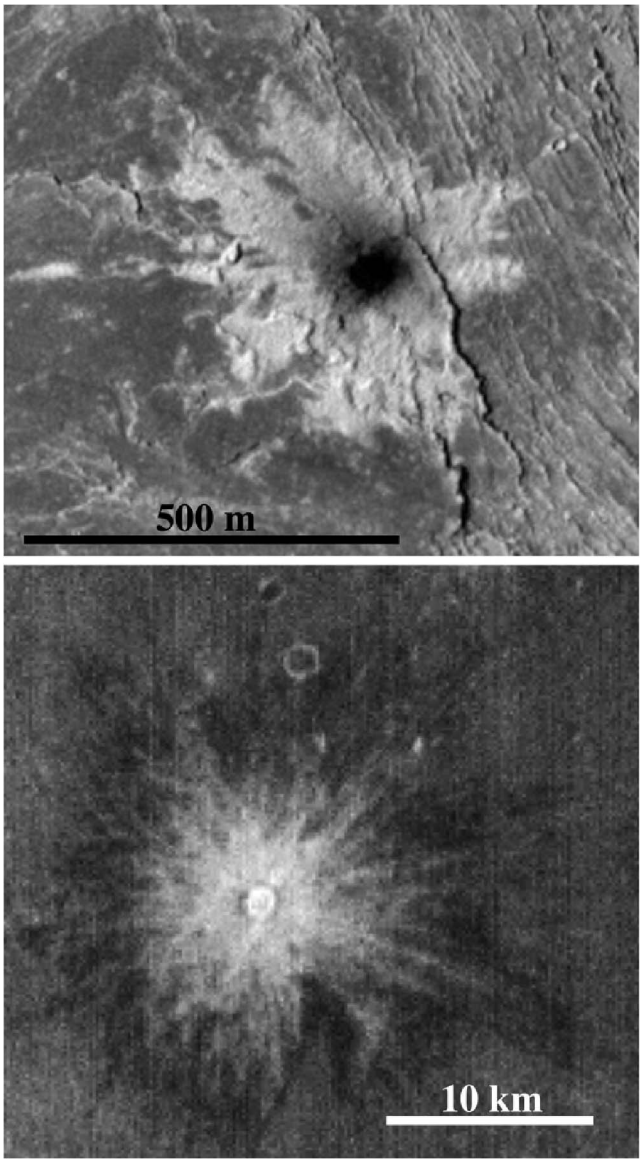

Fig. 3. Facies of fresh craters with bright ejecta on Mars. Shown at top is a visible image (part of M02-00581) of a ∼50-m diameter Zunil secondary and at bottom is part of a THEMIS nighttime IR image of a 1.5-km diameter crater (not a Zunil secondary, but a crater large enough to show morphologic details at 100 m/pixel). These craters have interiors that are dark and rocky (warm at night), near-rim ejecta that are moderately dark and rocky, and distal ejecta that are bright and fine-grained (cool at night).

Daytime and nighttime THEMIS mosaics of the Athabasca Valles region were acquired and assembled to support the study of this region as a candidate landing site for MER (Christensen et al., in press; McEwen et al., 2002). The nighttime mosaic revealed roughly east–west trending streaks of cold material superimposed over diverse terrains (Fig. 5). Small bright (warm) spots are resolved in some cold streaks. Comparison to MOC images reveals a 1:1 correspondence between these streaks and concentrations of the small bright-ejecta craters (Fig. 6). The bright ejecta is especially cold at night (dark in thermal-IR images) and the interiors of the largest secondary craters form relatively warm (bright) spots in nighttime THEMIS IR images. The streaks are composed of clusters of secondary craters, much like those first observed by Ranger imaging of rays from Tycho (Shoemaker, 1965).

A larger-scale nighttime IR mosaic of the Cerberus region was assembled and shows a regional pattern to the cold streaks: they radiate from a position ∼400 km east-southeast of Athabasca Valles (Fig. 7). THEMIS daytime IR and visible images revealed the fresh, 10.1-km diameter crater Zunil at this central location (7.7° N, 166° E). A THEMIS visible image at 18 m/pixel and MOC images at 3.1 m/pixel (Fig. 8) show Zunil to be pristine, with no superimposed impact craters resolved. A total of 4 complete MOC images over Zunil have been released to date (R08-02140, R11-03468, R12-0-2652, R15-00138), and none shows a definite impact crater superimposed on the continuous ejecta blanket or the crater interior. Portions of the crater floor are heavily pitted, but the pits lack raised rims or ejecta blankets indicative of impact origin. According to the HPF or NPF a crater ⩾24 m diameter (easily resolved in MOC images) should occur every 2–8 Ka over an area the size of the Zunil interior and continuous ejecta (∼600 km^2). However, we do not believe that Zunil is younger than 10 Ka, as discussed later in Section 4.4.

Unlike typical secondary crater fields (e.g., Melosh, 1989), Zunil does not have obvious chains of elongated secondary craters within ∼16 crater radii (80 km) of the rim (Figs. 8 and 9). The great majority of the resolved craters formed from blocks thrown from 20 to at least 300 crater radii, impacting with velocities sufficient to produce at least crudely circular craters. The largest Zunil secondary identified to date is only 230 m in diameter, located at 8.9° N, 164.8° E, about 105 km from Zunil (MOC image M08-02523). Typically the largest secondary is ∼5% the size of the primary (Melosh, 1989), which would be ∼500 m for Zunil, but we see no evidence for a crater this size near Zunil. A few blocks up to 15 m diameter are seen on the near-rim ejecta (Fig. 8), and many dark specks are probably boulders just below the image resolution, or smaller than ∼6 m in diameter for the 3-m/pixel images. Layering seen in the crater wall suggests that the stack of lava flows is at least a few hundred meters thick in this region. The paucity of large blocks near the rim suggests that most of the target material broke up into blocks smaller than ∼6 m in diameter, perhaps corresponding to the spacing of cooling joints in the basalts. Those blocks both smaller than 6 m and ejected at low velocities may have failed to make resolvable craters within 80 km of Zunil.

Zunil produced ejecta flow lobes (Fig. 8). The crater should have excavated to a depth of roughly 400–700 m [based on scaling relations described by Schmidt and Housen (1987) and Melosh (1989, p. 78)], so the flow ejecta suggests ground ice was present within this depth range when the crater formed (e.g., Stewart et al., 2001). Since this crater may be only a few Ma or less in age, the shallow ice is probably still present. Zunil resides downstream of “Gro-

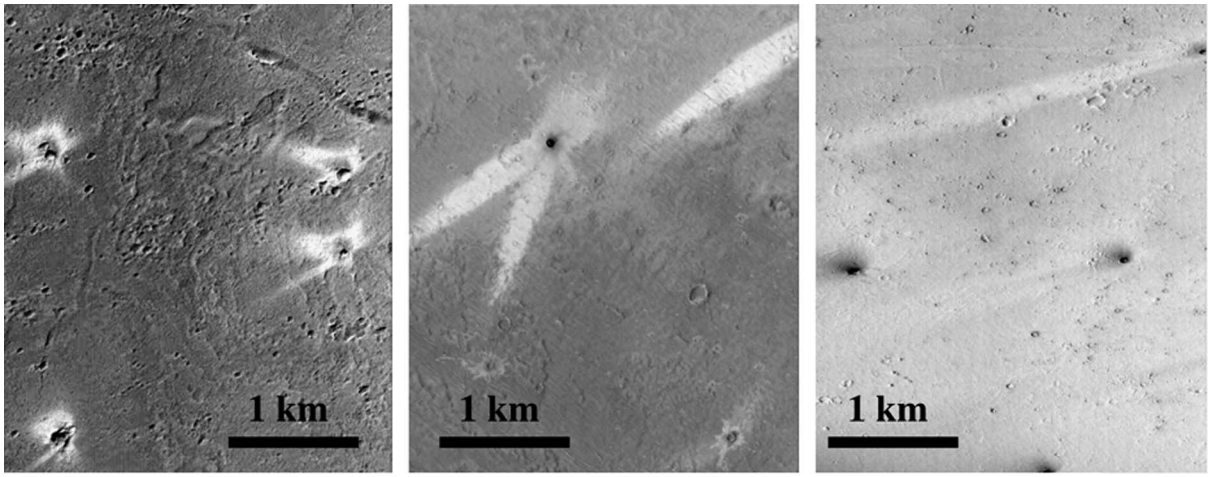

Fig. 4. MOC images showing wind erosion of the bright ejecta from Zunil secondaries, increasing to the east and north from Zunil. Left: M02-001397 at 7.1° N, 165.2° E (just SW of Zunil). Middle: E16-01783 at 13.5° N, 167.6° N (NE of Zunil). Right: M03-06217 at 6.2° N, 172.2° E (SE of Zunil). All 3 images are ∼6 m/pixel and 3 km wide. The bright ejecta has been modified into bright streaks following prevailing winds, and increasingly modified from west to east.

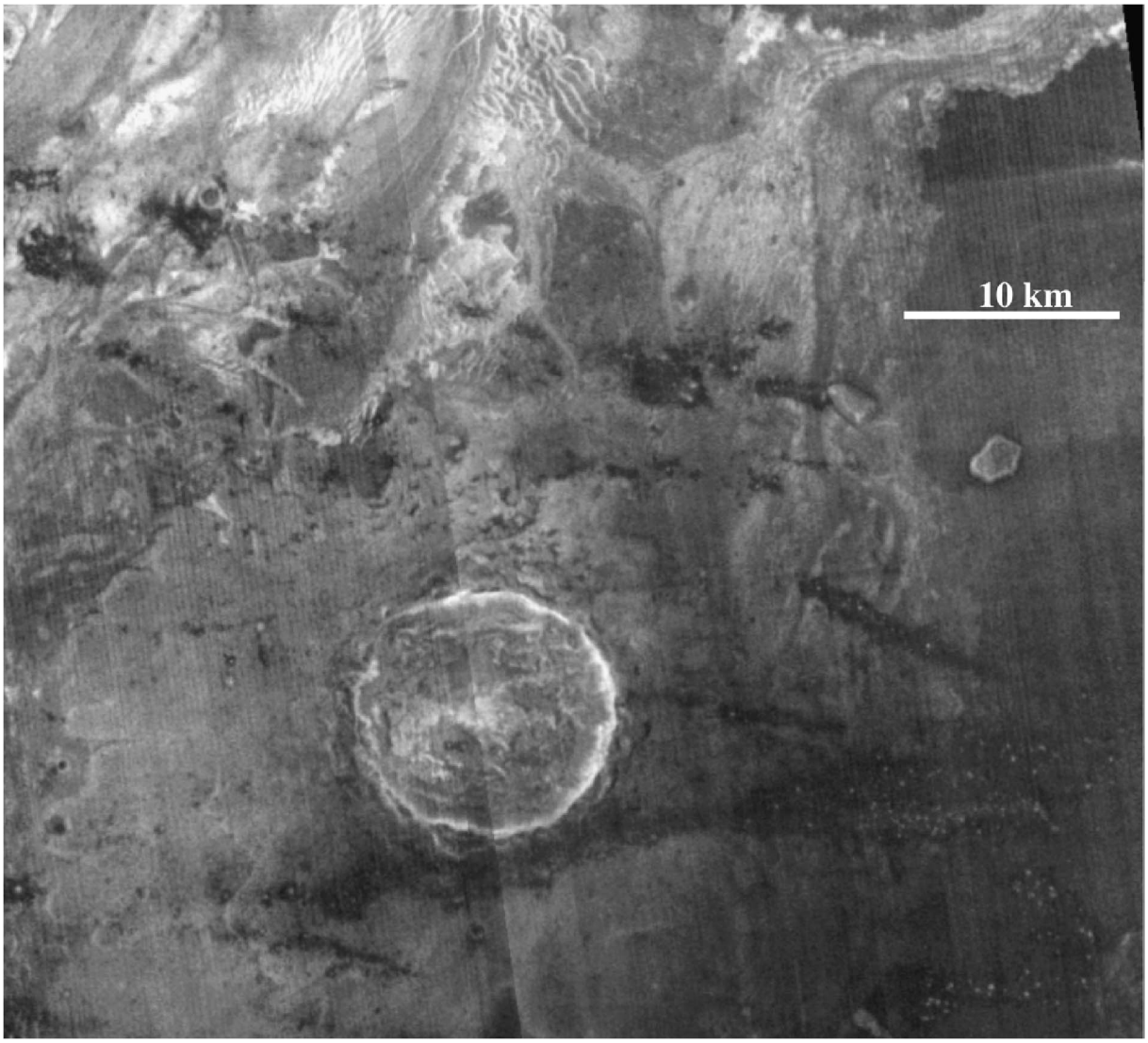

Fig. 5. Part of a mosaic of THEMIS IR images (nighttime) of the Athabasca Valles region, showing dark (relatively cool) streaks (Zunil rays) with bright (warmer) spots (interiors of larger Zunil secondaries). The scene is about 50 km wide; located SE of Athabasca Valles. North is up.

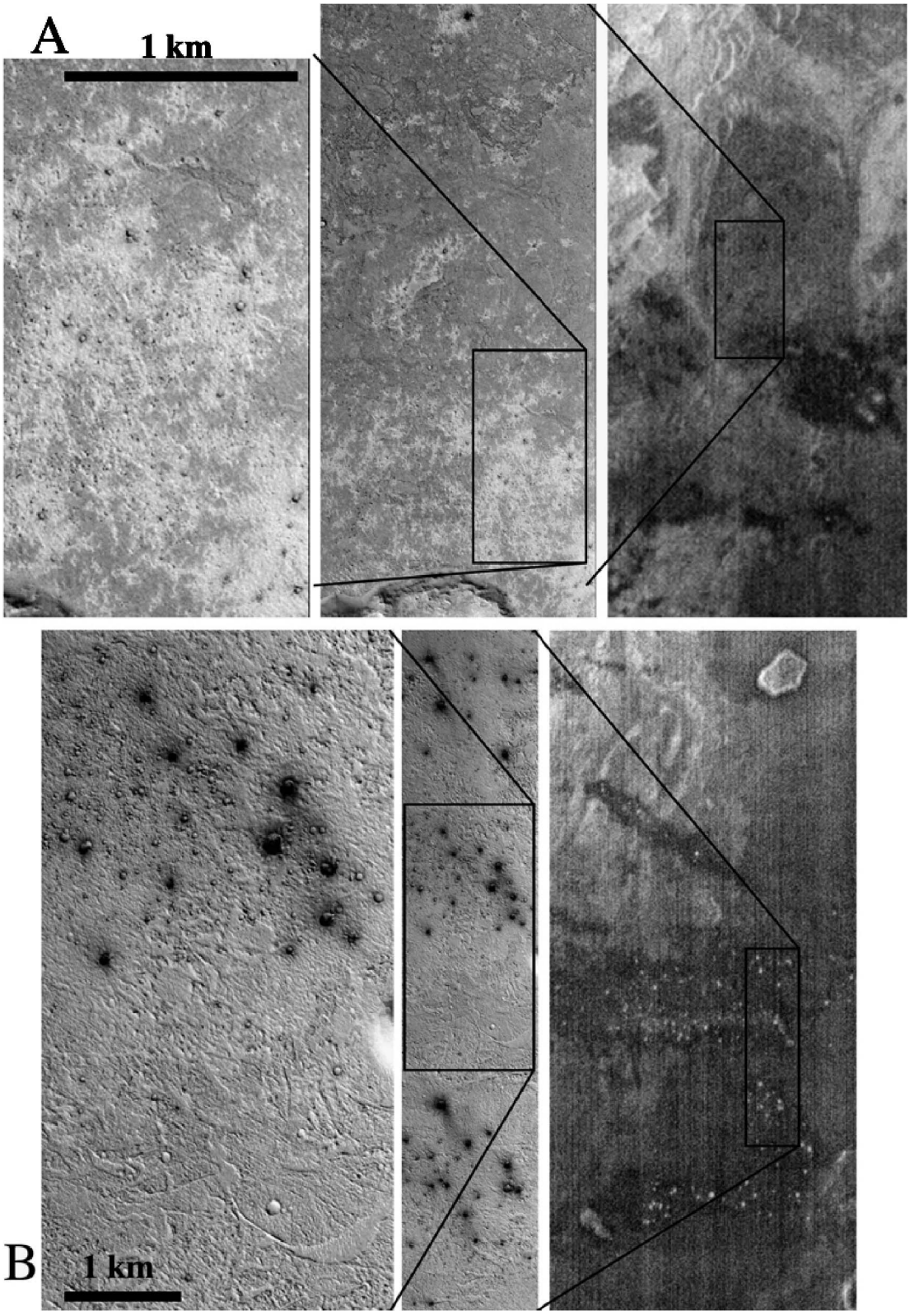

Fig. 6. THEMIS-MOC comparisons, showing that the dark (cool) rays seen in THEMIS nighttime IR images correspond to streaks and clusters of fresh secondary craters seen in MOC images. (A) THEMIS image I00825008 (right) and MOC image E1201123 (middle and left) at 9.3° N, 156.8° W. (B) THEMIS image I0261000 (right) and MOC image E1100508 (middle and left) at 8.3° N, 157.3° E. Full MOC image width in the middle of both A and B is 3 km. Note that the bright ejecta of secondaries seen in (B) blend into the bright (dusty) background in the visible MOC image but are still distinctive in the THEMIS nighttime image.

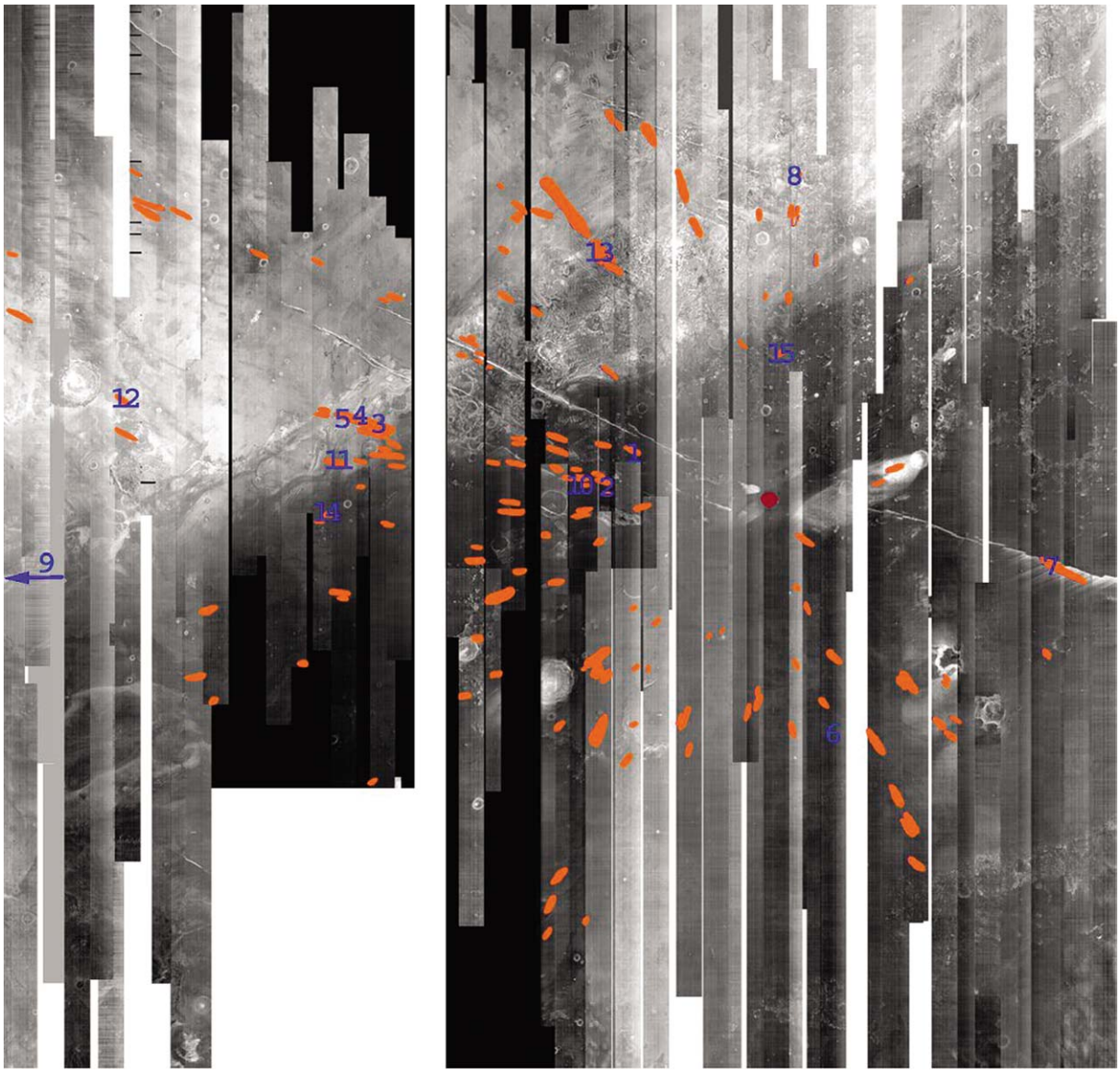

Fig. 7. Mosaic of THEMIS nighttime IR images showing Zunil rays (in orange) that can be identified from this mosaic. Zunil is marked by a red dot near right center and the numbers correspond to locations of images used for crater counts (Table 2). This is an uncontrolled mosaic in the raw image geometry, so north is ∼7 degrees to the right of up. The area covered ranges from about 172° E to 153° E and 6° S to 18° N. The most distal ray shown here is ∼1100 km from Zunil, but there are isolated rays up to 1600 km away that are oriented radial to Zunil.

ta' Valles" (provisional IAU name) described by Burr et al. (2002a) and Plescia (2003), which could have recharged the ground ice in recent geologic time.

We mapped out rays that could be identified from THEMIS nighttime IR images (Fig. 7). The secondary craters extend in all directions from the primary, although they are more difficult to detect to the northeast and east of the primary where the dust mantling appears to be thicker and eolian processes are redistributing the fine ejecta of the secondary craters (Fig. 4). However, the identifiable secondary craters and rays are asymmetric, extending 1600 km to the west-southwest (M08-00352), but only 470 km to the east (THEMIS image V08008021) and 390 km to the north (E12-03443). This asymmetry can be explained by moderately oblique impact from the east-northeast (Artemieva and Pierazzo, 2003). More detailed mapping of the rays is in progress (Preblich et al., 2005).

2.2. Counts of secondary craters

We estimated the total number of Zunil secondaries in two ways. First, we counted small craters over four regions of the channel floor of Athabasca Valles (we selected the four images without regard to the positions of rays; Table 1), and put each crater into one of 3 categories:

(1) those with the TI/albedo facies described above for recent craters and clearly associated with rays radial to Zunil,

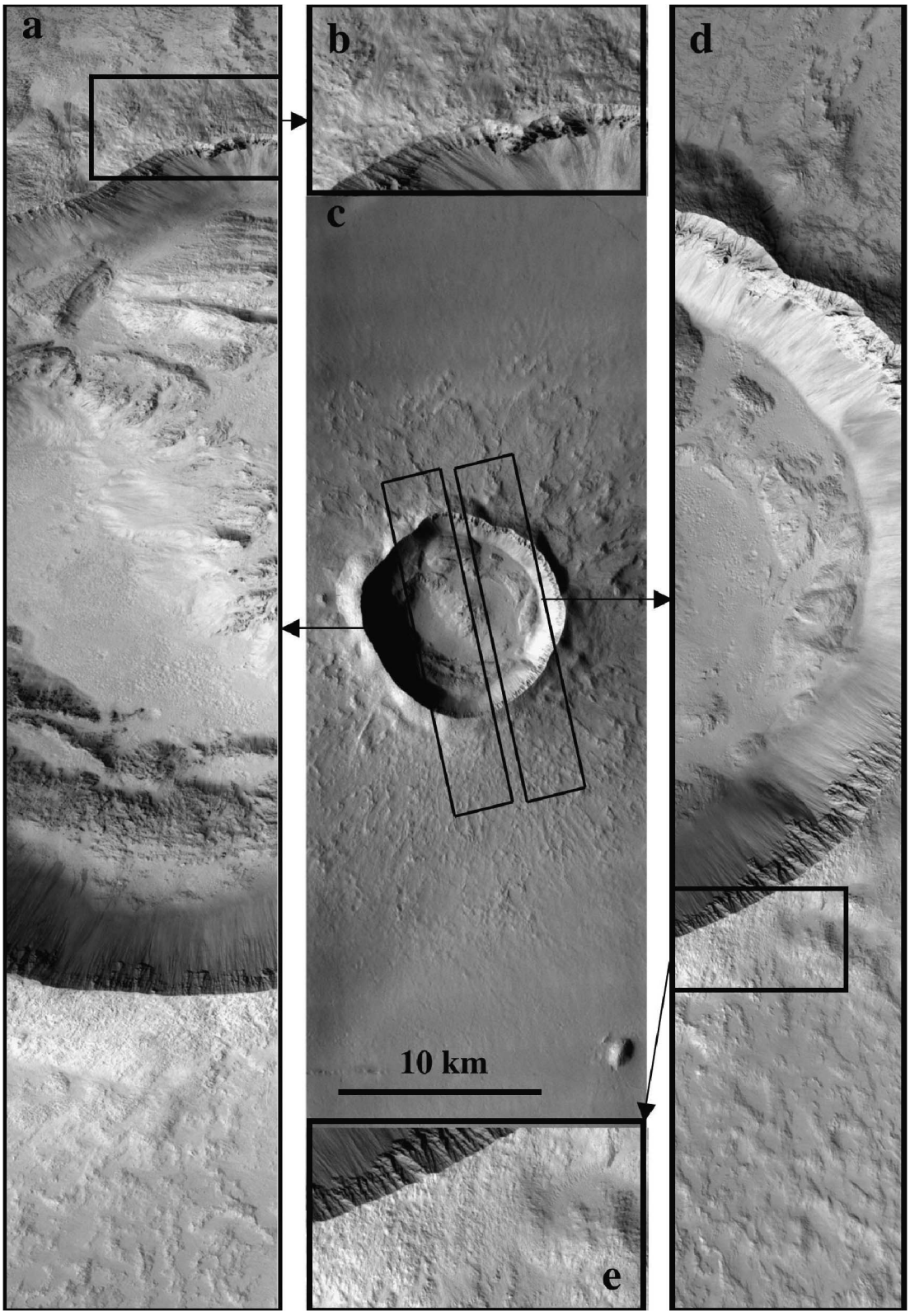

Fig. 8. High-resolution images of Zunil. In the center (c) is THEMIS visible image V09818024 at 18 m/pixel, simple-cylindrical map projection (north is up). Image swath is 18 km wide; Zunil's average diameter is 10.1 km. Part of MOC image R1500138 (3 m/pixel) is shown in (a), and part of R0802140 (3 m/pixel) is shown in (d). Panels (b) and (e) are enlargements showing blocks on the crater rim.

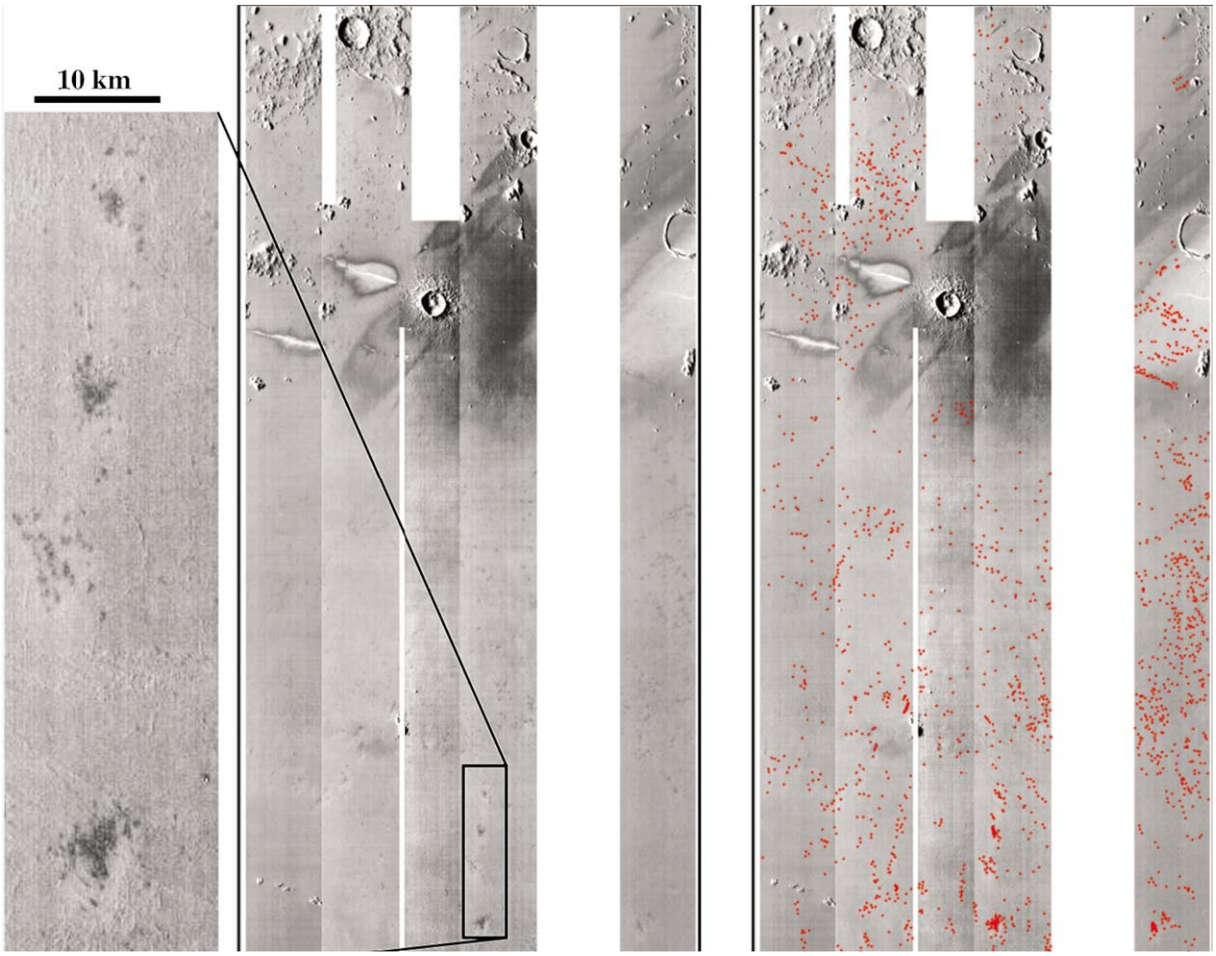

Fig. 9. Mosaic of THEMIS daytime images over a region including Zunil (upper-center). Middle image shows original data, with a blowup of part of I01879005 at the left showing clusters of secondary craters, which are dark (cool; relatively high TI) spots. At right is the mosaic with some of the large secondary craters (those identifiable at 100 m/pixel) marked with red dots. North is ∼7 degrees left of up. Mosaic scene is ∼180 km wide.

Table 1
Craters (∼20–100 m diameter) superimposed over Athabasca Valles

MOC image	Resolution (m/pix)	Number of craters	Area counted (km^2)	% Inside rays	% Bright-ejecta craters
M0700614	5.9	163	78	71	77
E1002604	5.9	18	33	56	67
M0200581	5.9	148	57	78	85
M0201973	5.9	51	45	80	87
Total		380	213	73	80

(2) those that do not have the recent facies, and
(3) those that have the recent facies but are not clearly part of rays.

We interpret (1) as very likely secondaries from Zunil, (2) as craters probably not associated with this event, and (3) as probably from Zunil, given that these craters are very distinctive and quite rare over other regions of Mars (Robert Strom, personal communication, 2002–2004). 73% of the 380 craters we counted are in category (1), 20% are in (2), and 7% are in (3). We conclude that ∼80% of the craters superimposed over the floor of Athabasca Valles originated from this single impact event. The area counted covers 213 km^2, 0.01% of the area of a circle with 800 km radius (the approximate average radial extent of well-defined rays and Zunil secondaries). If this density is typical of the secondary craters within this circular area, then there should be a total of 3×10^6 secondary craters ∼20–100 m in diameter. The rays appear denser than average over these portions of Athabasca Valles, but they are best seen over terrains such as this with relatively high thermal inertia (Preblich et al., 2005) so this may be representative of cratering. The number of small craters was probably underestimated due to resolution limits and saturation-equilibrium in dense portions of the rays, but we nevertheless have an order-of-magnitude estimate of 10^6 secondary craters larger than 20 m in diameter.

We derived a second estimate following a different approach using 15 different MOC images distributed more widely around Zunil (Table 2). All craters larger than four pixels in diameter were counted, but separately for those outside or within rays defined by the THEMIS IR mosaics (Fig. 7). From this approach we include craters that may be Zunil secondaries but lack the bright ejecta, perhaps re-

Table 2
Zunil secondary crater counts

# In Fig. 7	MOC image number	Scale (m/px)	# Craters	Area (km^2)	Inside or outside ray?	% Bright-ejecta craters	Best-fit $\log N/\text{km}^2$	Distance (direction) from Zunil	N ($\geqslant$10 m)/km^2
1	E0501457	5.89	430	17.7	Inside	~56%	$-2.65\log D + 4.94$	178 km (W)	205
2	E1104266	4.63	206	5.1	Outside	~7%	$-3.68\log D + 7.01$	209 km (W)	
3	M0701888	5.87	268	23.3	Inside	~94%	$-3.06\log D + 4.78$	557 km (W)	47
4	E1101849	3.09	117	7.6	Inside	~84%	$-5.50\log D + 7.27$	575 km (W)	27
5	M0700614	5.87	177	8.9	Inside	~92%	$-4.07\log D + 6.35$	606 km (W)	125
6	M1301528	5.79	215	9.3	?	~23%	$-2.85\log D + 5.23$	333 km (SE)	
7	M0801960	2.92	252	6.4	Inside	~84%	$-4.71\log D + 6.77$	414 km (E)	63
8	E1203443 top	6.22	306	15.8	Inside	~25%	$-3.53\log D + 6.15$	391 km (N)	321
8	E1203443 bottom	6.22	171	7.8	Inside	~12%	$-4.42\log D + 7.51$	391 km (N)	731
9	M0201393	4.37	92	8.5	Outside	~0%	$-0.59\log D + 1.34$	1771 km (W)	
10	E0902413	3.09	268	2.3	Inside	~75%	$-3.30\log D + 5.00$	231 km (W)	42
11	E0503124	4.41	87	3.6	Inside	~82%	$-3.17\log D + 4.68$	602 km (W)	28
12	SP121904	6.95	172	16.9	Inside	~83%	$-4.98\log D + 7.26$	859 km (W)	98
13	M0401407	5.90	303	6.6	Inside	~95%	$-4.63\log D + 7.15$	408 km (NW)	186
14	E0201207	2.95	139	2.1	Inside	~78%	$-3.14\log D + 4.93$	621 km (W)	54
15	M2001848	5.90	462	11.8	Inside	~78%	$-2.78\log D + 4.67$	234 km (N)	77

moved by eolian or ray-forming processes from the smallest craters. We find a steeper SFD (b up to 5.5) inside the rays and a flatter SFD ($b \sim 2$) outside the rays, whereas previous measurements of small craters in this region (Hartmann and Berman, 2000; Burr et al., 2002a) showed intermediate SFDs, perhaps from a mixture of Zunil secondaries and other small craters. The craters reach saturation equilibrium ($b \sim 2$) within some of the rays, reducing the overall SFD slope. The best-fit slopes in Table 2 vary widely, probably due in part to the small range of crater diameters, ~20 m (resolution limit) to ~100 m diameter. The best-fit slopes were derived from weighted fits to differential counts (Chapman and Haefner, 1967); we subtracted 1 to give b.

From the images inside rays the average density of craters $\geqslant$10 m in diameter is 154 per km^2 (right-hand column of Table 2, estimated from the weighted fits). From our mapping (Fig. 7) rays cover ~3% of an 800-km-radius circle centered on Zunil, so we estimate a total of 0.95×10^7 craters with diameters of 10 m or larger. From the counts of bright-ejecta craters outside of rays (Table 1) we can increase this estimate by ~10%, although many of the smallest Zunil secondaries may have lost their bright ejecta so this is a lower limit. We are underestimating the number of craters in regions of saturation equilibrium, but have not attempted a correction. In addition, we expect ~70% of the secondaries to fall at ranges greater than 800 km (see Section 3.1). Thus our total estimate of Zunil secondaries $\geqslant$10 m in diameter is 3.5×10^7. We assume a value of 1×10^7 for comparable craters in our modeling exercise in Section 3.2, but extend this to 10^8 secondaries from larger primary craters. The number of secondaries $\geqslant$20 m in diameter is of order 10^6, in agreement with the estimate from Athabasca Valles.

Is it physically plausible for a 10-km primary crater on Mars to create 10^7 craters 10–230 m in diameter? Yes, as demonstrated by 3D hydrodynamic modeling (Section 3.1) in which a simulated Zunil impact ejects 1.5 km^3 of rocks (~5% of total ejecta) at >1 km/s. This high-speed ejecta is broken into 6×10^8 fragments with momentum sufficient to produce secondary craters $\geqslant$10 m in diameter. The amount of ejecta that produces secondary craters ranges from 0.2% to 7.5% of the material excavated from the primary craters in Table 6.1 of Melosh (1989), although these estimates ignore distant secondaries.

2.3. How unusual is Zunil?

A search of the THEMIS and MOC data over Amazonian and Late Hesperian plains has revealed a few other morphologically pristine large ($\geqslant$10 km) craters that may have produced large numbers of distant secondaries (e.g., Mouginis-Mark et al., 2003), but none with preservation of rays and the fine outer ejecta facies in the secondary craters. However, Tornabene et al. (2005) report the identification of four rayed craters with diameters of 7.4, 6.9, 3.3, and 2.0 km, and two other candidates with faint rays. The rays of these craters extend up to 600 km and have thermophysical properties similar to those of Zunil. Four of these craters are in Elysium Planitia and the other two are south of Tharsis. Zunil rays are only clearly visible on the THEMIS nighttime images over regions of moderate thermal inertia and high albedo, consistent with thin dust coatings over rocky substrates (Preblich et al., 2005). All six of the other rayed craters are also located over regions of Mars with moderate thermal inertia but a bright albedo, along the margins of the regions of high dust-cover index (Ruff and Christensen, 2002) and low thermal inertia, so perhaps this type of surface is needed to form and/or preserve the rays. Roughly 10% of Mars' surface has these characteristics; on ~20% of Mars an impact could occur with 500 km rays that would cross this kind of surface. This suggests that Zunil is the youngest crater $\geqslant$10 km in diameter on ~20% of the martian surface. We expect ~1 crater $\geqslant$10 km per 10^6 yrs on all of Mars (Ivanov, 2001), so Zunil may be less than a few (~5) Ma old.

Clearly Zunil is especially young for a crater of this size, but is it otherwise unusual? As discussed above it appears unusual because it has few large secondary craters within ∼16 radii. Other large craters on Mars also have few secondaries within ∼10 crater radii (Schultz and Singer, 1980; Barlow, 2003), so perhaps these are other examples where most of the secondaries formed at greater ranges.

The most important question for this paper is whether the number of secondary craters produced by Zunil is unusually high. Our estimate for Zunil is ∼2 orders of magnitude greater than estimates of secondaries from lunar craters, but there were image resolution and other limitations in these estimates (Shoemaker, 1965; Wilhelms et al., 1978). From the spallation model of Melosh (1984; Head et al., 2002) we expect impacts into competent targets with little regolith to produce the highest number of distant secondaries. So, the Cerberus Plains, the youngest large-scale lava plains on Mars, should be ideal terrain for the production of distant secondaries. However, the regolith layer has been considered unimportant when thinner than the projectile radius, so a 200-m-radius projectile (producing a 6.7 km crater in the simulation of Head et al., 2002) would be insensitive to a regolith layer thinner than 200 m. Therefore, craters larger than just a few km should not be affected by the comparatively thin regolith over Hesperian and Amazonian terrains (see Section 4.3), although the near-surface bedrock may also tend to be less competent on older terrains. Zunil was probably not produced by an unusually high impact velocity (such as from a comet, >15 km/s), because that would cause more melting and a smaller volume of solid blocks would be ejected at high velocities (Section 3.1). In summary, we cannot rule out the possibility that the number of secondaries produced by Zunil is typical of impacts into martian lava plains of Hesperian or Amazonian age, or from large (>100 km diameter) craters over any terrain.

2.4. Is Zunil the source crater for some of the basaltic shergottites?

Zunil is an excellent candidate for one of two source craters for the known basaltic shergottites with emplacement ages of 165–177 Ma and ejection ages of ∼1.5 and ∼2.7 Ma (Nyquist et al., 2001). The ∼1.5 and ∼2.7 Ma ejection ages for the two groups of basaltic shergottites are both consistent with our arguments (above) that Zunil is less than a few Ma old. The Cerberus Plains lavas are probably composed of basalt according to the lava emplacement models and terrestrial analog studies of Keszthelyi et al. (2000, 2004b). There is also a basaltic spectral signature in TES data over small areas around the Cerberus Plains that are not obscured by dust (Bandfield et al., 2000). The near absence of craters larger than 500 m (probable primaries for this young terrain) superimposed on the youngest lavas indicates they are less than ∼100 Ma old (Lanagan and McEwen, 2003). There are clearly older lavas only tens of meters below the young lavas (Hartmann and Berman, 2000), so the presence of 165–177 Ma lavas near the surface is quite consistent with these crater dates. The basaltic shergottites probably cool within lava flows on the surface (Nyquist et al., 2001; Mikouchi et al., 2001) but there is a stack of lavas hundreds of meters thick in the Cerberus plains so we do not necessarily have samples of the very youngest lavas in the upper few tens of meters. However, the top lavas are the most likely to be ejected at greater than escape velocity (Artemieva and Ivanov, 2004), so we cannot rule out the possibility that the surface lavas around Zunil are 165–177 Ma old.

3. Models of secondary cratering

3.1. Hydrodynamic simulation of the Zunil impact

3.1.1. Parent crater ejecta modeling

This numerical modeling is similar to that for delivery of martian meteorites (Artemieva and Ivanov, 2004). Oblique impacts are simulated with a three-dimensional version of the SOVA code (Shuvalov, 1999), coupled to ANEOS-derived (Thompson and Lauson, 1972) equation of state (EOS) tables for granite (Pierazzo et al., 1997). We do not yet have a proper EOS for basalt, which means that particle velocities are systematically 0.2–0.4 km/s too high, and we slightly overestimated the amount of high-velocity unmelted ejecta. We use a tracer (massless) particle technique to reconstruct dynamic (trajectories, velocities), thermodynamic (pressure, temperature) and disruption (strain, strain rate) histories in any part of the flow. The pressure-ejection velocity distribution in the central cross-section of the flow, as reconstructed from the tracers, is shown in Fig. 10. The source of the fragments producing distant secondary craters is the region with velocity >1 km/s and pressure <50 GPa. The total volume of high-velocity solid ejecta is about 1.5 km^3 (∼5% of total ejecta of ∼30 km^3). About 0.18 km^3 of the simulated rocks are ejected from Mars.

Ejecta motion in an impact-disturbed martian atmosphere would be best described by multi-phase hydrodynamics (Valentine and Wohletz, 1989). Each particle would be characterized by its individual parameters (mass, density, shape, position, velocity) and exchange momentum and energy with a surrounding vapor–air mixture. Material disruption would be assumed to occur when the density of the solid or molten material drops below the normal density for a given temperature within a single computational cell (i.e., the material is subject to tension). However, it is impossible for us to describe each solid fragment separately due to computational limits (disruption of a single 50-m computational cell creates 1.25×10^5 m-sized fragments, or 1.25×10^8 10-cm-sized fragments). For this reason we use a simple representative particle technique (Teterev, 1999), i.e. a group of particles with similar sizes, velocities and initial positions are described by a single equation of motion, but the total quantity of particles is used to define the momentum and heat exchange with the atmosphere. The representative particle's initial position within the cell is randomly defined

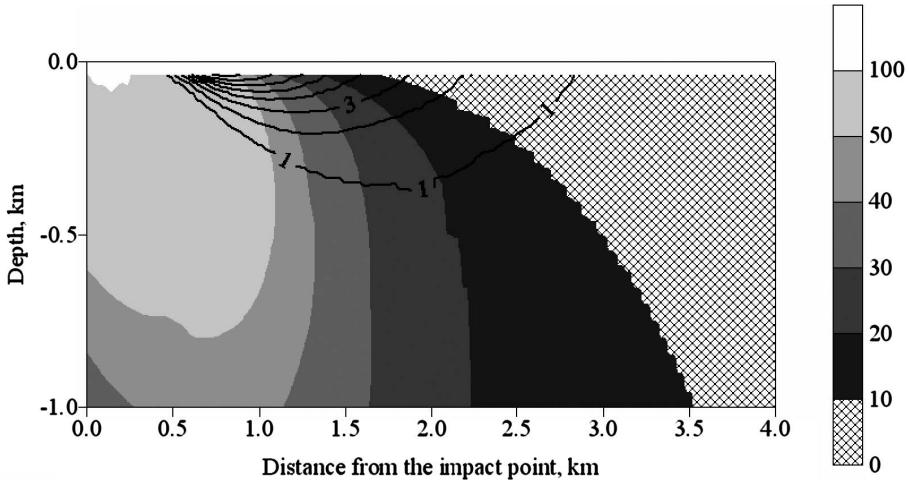

Fig. 10. Cross-section of the maximum pressure contours (gray scale; GPa) and ejection velocity contours (thick black lines; km/s) generated by a 1-km-diameter projectile striking the surface at the point (0, 0) at 10 km/s and at a 45° angle. The source of the fragments that produce secondary craters is the region above the 1 km/s velocity curve and less than 50 GPa pressure (so they remain solid).

and the hydrodynamic velocity at this point gives its initial velocity. All particles are treated as spherical, although the shape may differ substantially. Nevertheless, strongly asymmetric fragments rotate rapidly and may be represented, on average, as spheres.

The size of the fragments ejected at a given point at a given time depends on the material properties and on the process itself (strain, strain rate, etc.). The preferred approach is to implement a disruption process in the hydrocode (Melosh et al., 1992; Asphaug and Melosh, 1993; Head et al., 2002), but in this study we chose a simplified approach. The most likely fragment size to occur under loading at a constant strain rate, as well as fragment size distribution, is defined according to Grady and Kipp (1980) theory at the moment of disruption (strain of the order of 0.01–0.1). An average fragment size may also be associated with ejection velocity: $l_a = T D_{pr}/(\rho V_{ej}^{2/3} V^{4/3})$ (Melosh, 1984), where T is the tension at fracture (~0.1 GPa for basalt and other igneous rocks), D_{pr} is the projectile diameter (1 km for the Zunil simulation), ρ is the density of the target rocks (2.8–2.9 g/cm^3), V_{ej} is ejection velocity, and V is impact velocity (10 km/s). Or, the standard cumulative distribution of fragments $N = CM^{-b}$ (Melosh, 1989) may be used with the maximum size l_{max} defined by the value of maximum compression P_{max}: $P_{max}/P_0 = (l_0/l_{max})^{3\beta}$ (Shuvalov, 2002), where P_0 is the pressure near the crater rim, l_0 is the size of the largest excavated fragment, β is a Weibull exponent for the rocks, and β is 0.25 (Weibull, 1951). In this work, we consider all three methods [for more details see Artemieva and Ivanov (2004)]. The results are compared in Fig. 11. All three methods give reasonable results with the largest fragment ejected at high velocity (>1 km/s) of about 10–20 m.

Fig. 12 shows an overhead view of the growing crater 2 seconds after the impact. The earliest and the fastest ejecta are strongly asymmetric; later the ejection velocity drops below 1 km/s, the fragment size increases to ~10 m, and the ejecta is more symmetric. Note that many of the smallest fragments are ejected at velocities exceeding Mars' escape velocity (5 km/s), while those ejected at 1–5 km/s will fall back to form distant secondary craters.

3.1.2. Sizes of the secondary craters

As we expect rather small secondary craters (in the range 10–500 m), their size D_{cr} should be defined according to scaling laws for craters in strength or intermediate between strength and gravity regimes (Schmidt and Housen, 1987). To include both effects we use an approach described in Ivanov (2001), which implicitly includes the strength of the target rocks (a poorly known value, which depends on the scale of the event) using the value of crater size that defines the strength-gravity transition, D_{sg}:

$$\frac{D_{cr}}{D_{pr} V^{0.55}} = \frac{1.21}{[(D_{sg} + D_{cr})g]^{0.28}}.$$

The value of D_{sg} may be defined from the crater morphometry (Moore et al., 1974; Pike, 1977; Housen et al., 1983). It is in the range of 300–600 m for the Moon corresponding to an effective target strength of less than 3 MPa (Melosh, 1989). Vickery (1987) used the higher value of 10 MPa. As D_{sg} is inversely proportional to gravitational acceleration, we use the value of 130–260 m for Mars. This means that only a few of the very largest Zunil secondaries might not have formed in the strength regime.

The most probable median angle for secondary impacts is 45 degrees. This impact angle leads to a decrease of crater size according to experimental data by Gault and Wedekind (1978): $D_\theta = D_{90} \sin^{2/3}\theta$, where θ is the impact angle measured from horizontal. Estimated values of secondary crater diameters for different impact velocities and for two values of target strength are shown in Fig. 13, which illustrates that the uncertainty in the crater size estimates is less than a factor of two.

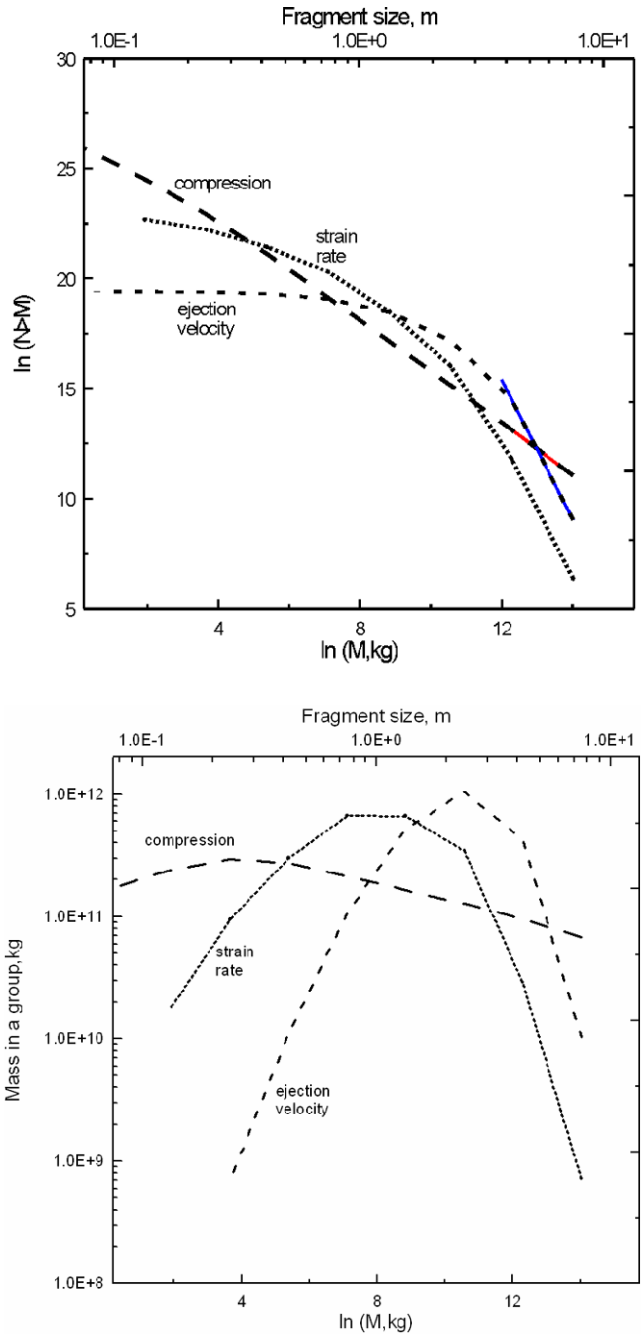

Fig. 11. Cumulative (upper plot) and differential (lower plot) size and mass distribution of ejected fragments. Three different methods have been used to derive these distributions: (1) the maximum fragment size is defined by the maximum compression and the SFD is $N = Cm^{-0.8}$ (Shuvalov, 2002)—long-dashed lines; (2) the maximum size is defined by the ejection velocity and the SFD is the Grady–Kipp distribution for basalt (Melosh, 1984; Grady and Kipp, 1980)—dashed lines; (3) the maximum size is defined by the strain rate value, the SFD is Grady–Kipp (Asphaug and Melosh, 1993)—dotted lines.

Crater size needs to be defined by a special method in the case of impact by a fragment swarm (Schultz and Gault, 1985). The crater diameter in this case is, approximately, $D_{\rm cr}^{\rm cl} = D_{\rm cr}(D_{\rm pr}/D_{\rm cl})^{0.18}N^{0.33}$, where $D_{\rm cl}$ is the clump diameter and N is the number of particles with diameter $D_{\rm pr}$ in the clump. In the present model we do not include overlapping or composite craters created by a clump of fragments that has not dispersed by the time of impact. Instead each ejected fragment creates a separate crater, which gives the upper limit to the number of secondary craters.

We have another modeling problem in how to describe the distribution of craters created by the "representative" particle and the "represented" particles of the same size moving along the same trajectories with the same velocities. In other words, we want to describe the distribution of craters created by multiple particles of similar sizes moving along similar trajectories with similar velocities. These particles will probably strike the surface as a loose cluster or as widely separated fragments. The "tightness" depends on the conditions at the moment of disruption, as there is a velocity gradient within the computational cell and the velocities of the fragments from each cell may differ substantially. We assume a velocity gradient of 100 m/s (which is less than 0.1 of the ejection velocity above 1 km/s), producing a dispersion of real fragments at the site of impact of $2V_{\rm ej}/g\Delta V_{\rm ej}$, i.e. ∼50 km.

The SFD of the simulated secondary craters is shown in Fig. 14, along with the NPF for the cumulative number of martian craters produced globally in 1 Ma. An "X" marks our estimate for the number of Zunil secondaries ⩾10 m diameter, about 100 times fewer than in the upper-limit simulation. The NPF predicts an intermediate value for N (⩾10 m) for craters produced globally in 1 Ma. We expect ∼one 10-km impact per Ma on Mars, but we also expect $\sim 10^2$ craters larger than 1 km, each of which would produce additional secondaries.

The spatial distribution of simulated secondary craters is shown in Fig. 15. There are artifacts due to model simplifications, such as only considering particles ejected at >1 km/s and the use of groups of represented particles, but the purpose of this simulation is to get a first-order result for the expected distribution of crater sizes as a function of range. 10–20 m craters are found at distances up to 3000 km, while craters larger than 50 m are found at distances less than 1000 km. The great majority of the secondaries are in the downrange direction from the parent crater. There are no rays because we have not attempted to model their formation.

An important result from this simulation is that we can predict what fraction of the secondaries are high-velocity background secondaries that may be nearly indistinguishable from primary craters. These data are summarized in Table 3. The startling result is that 96% of the craters form more than 400 km from the primary, which is farther than secondaries can usually be recognized, except when in rare well-preserved rays. ∼70% of the craters are predicted to form more than 800 km from the primary. Clustered impacts would be most common close to the primary (due to less time for dispersion), increasing the percentage of isolated craters at larger distances. This result supports the hypothe-

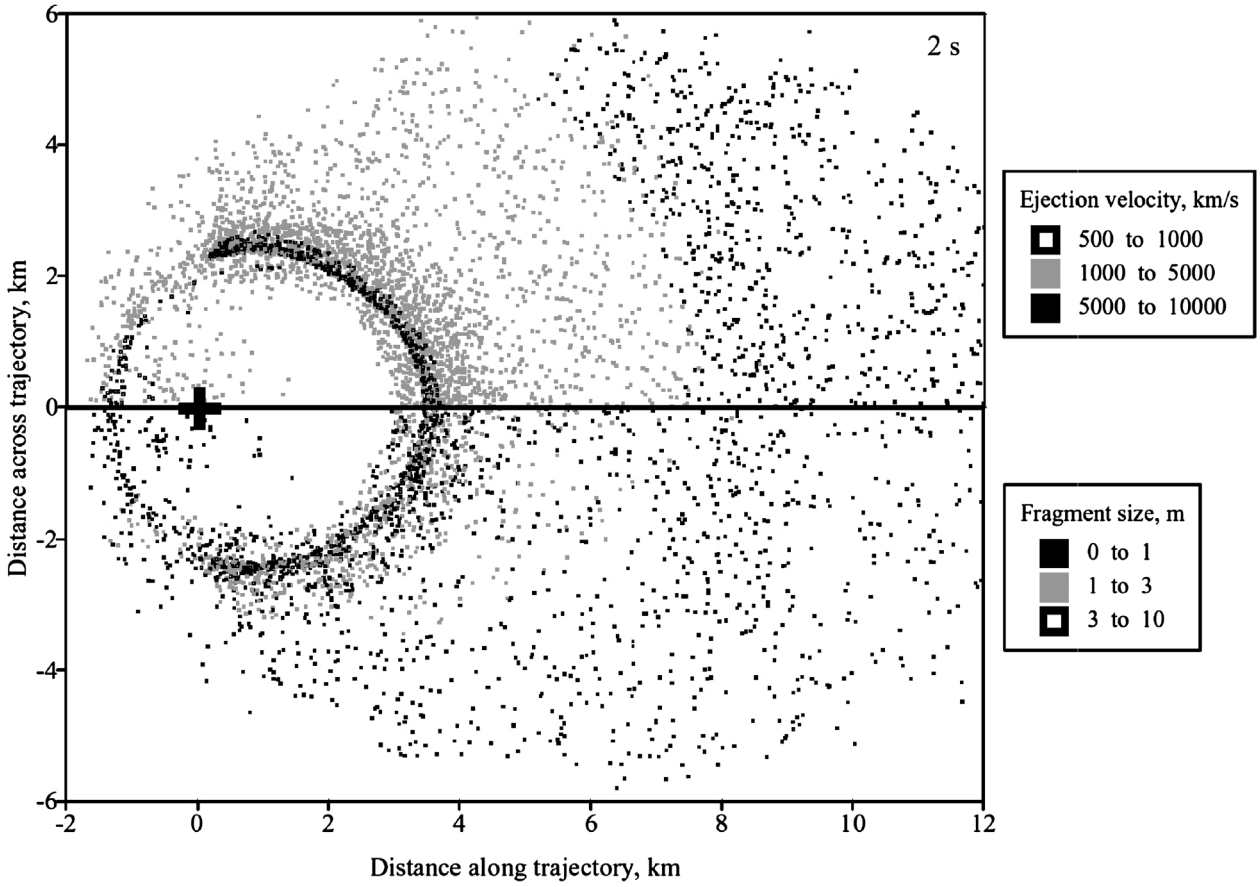

Fig. 12. Map view of the velocities and sizes of the fragments ejected from the growing crater 2 s after impact, for a simulation of a 1-km-diameter, 10-km/s projectile striking at the point (0, 0) from left to right. The upper half shows ejection velocity and the lower half shows fragment sizes.

Table 3
Number of secondary craters as a function of diameter and distance from the primary crater, as predicted from the hydrodynamic simulation

Diameter (m)	Distance					
	0–200 km	200–400 km	400–800 km	800–1600 km	1600–3200 km	>3200 km
1–10	2×10^3	8×10^3	1×10^4	1×10^4	2×10^4	1×10^4
10–20	5×10^5	2×10^7	1.6×10^8	2.6×10^8	1.5×10^8	1×10^7
20–50	7×10^5	4×10^6	6×10^6	4×10^7	4×10^6	5×10^4
>50	1×10^4	1×10^4	1×10^5	2×10^3	0	0
% of total	0.2%	3.8%	25%	46%	23%	2%

sis of Shoemaker (1965) that there can be huge numbers of distant secondaries.

3.2. Models of the global average production functions for secondary craters

To better understand small craters on Mars we modeled the global production of distant secondary craters as a function of primary crater production, with the assumptions that Zunil is typical and that production of secondaries scales with primary crater diameter. This model may be close to an upper limit to the actual production of distant secondary craters on Mars since Zunil appears to be an especially efficient producer of secondary craters [in agreement with Head et al.'s (2002) simulations of cratering in a competent target]. On the other hand, most secondaries result from primary craters larger than Zunil and could create even greater numbers of secondaries. We compare our model to those of previous workers (Shoemaker, 1965; Soderblom et al., 1974) in Table 4. The key parameters are the production function for large primary craters, the diameter of the largest primary, the SFD of secondaries, the largest secondary as a fraction of the primary diameter, and the cutoff on the number of secondary craters per event. Shoemaker (1965) modeled only 100,000 secondary craters per primary crater, based on the number of secondaries larger than 300 m estimated for Tycho, although he realized that this was limited by spatial resolution of the available images. This arbi-

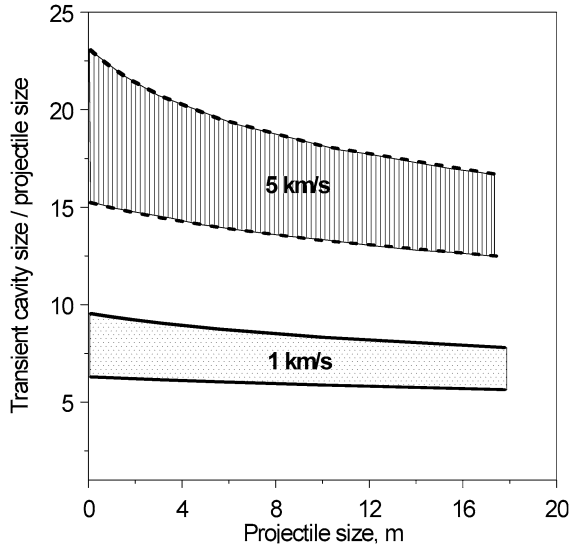

Fig. 13. The ratio of transient cavity size to projectile diameter for a given projectile size, primarily in the strength regime of crater growth. Impact velocities shown are 1 and 5 km/s (maximum impact velocity for secondaries on Mars). Gravity is also included, so the ratio slightly decreases with increasing projectile size, whereas in the pure strength regime the ratio of crater diameter to projectile diameter is constant. Two curves for each velocity restrict minimum and maximum estimates of the transient cavity diameter: the minimum corresponds to an oblique impact at 45° and a high target strength value (a strength–gravity–transition crater diameter $D_{sg} = 260$ m, roughly corresponding to a strength value $Y = 0.003$ GPa, Melosh, 1989); the maximum corresponds to a vertical impact and a lower target strength ($D_{sg} = 130$ m—inverse scaling with gravity from the lunar value of 300 m from Moore et al., 1974).

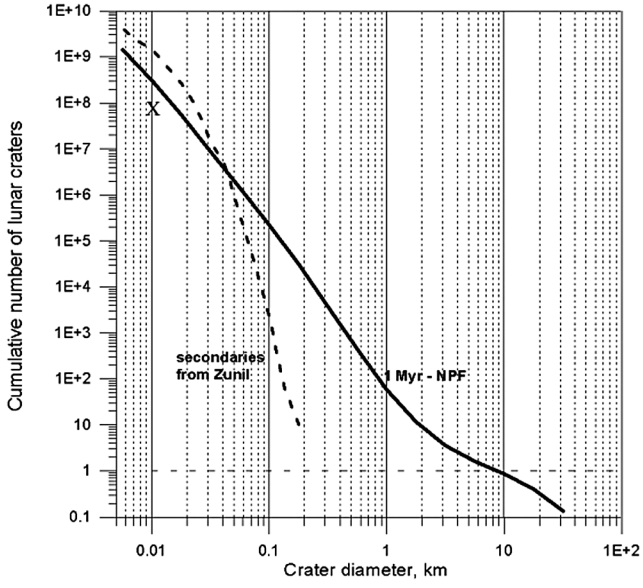

Fig. 14. Cumulative numbers of craters on the whole martian surface accumulated over 1 Ma based on the NPF (solid line). The dashed line represents secondaries predicted from the Zunil-like impact simulation. The best fits are $N \sim D^{-3.2}$ for the range 10–30 m, and $N \sim D^{-10}$ in the range 50–150 m. "X" marks our estimated number of actual Zunil secondaries. Zunil alone may account for all of the 10-m size craters predicted by the NPF, but primary craters smaller than 10 km in diameter (of which ~50 are predicted by the NPF over 1 Ma) would also contribute secondary craters in the 10-m size range.

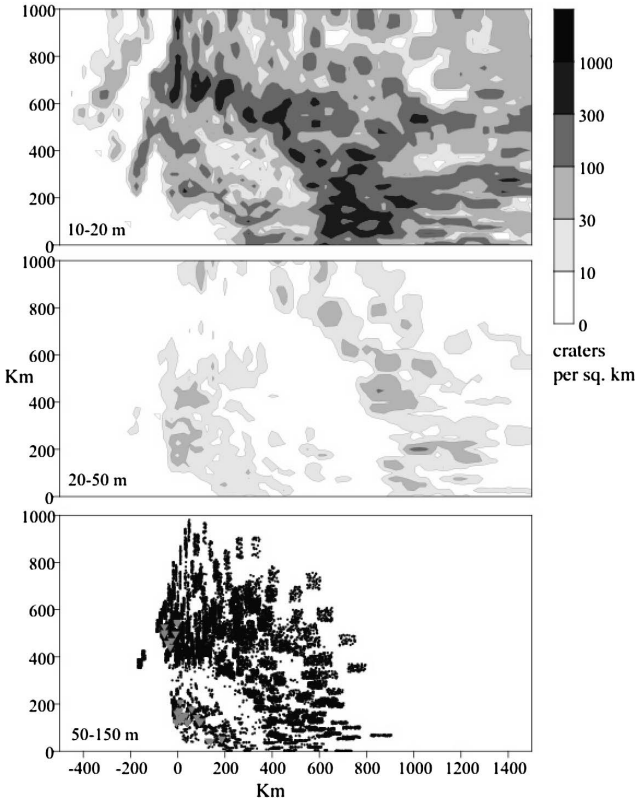

Fig. 15. Surface density (craters/km^2) predicted by the model for secondaries with 10–20 m diameter (top) and 20–50 m diameter (middle). Bottom plot shows all craters 50–100 m diameter (black dots) and >100 m diameter (grey triangles). Discontinuities at certain distances from the point of impact are artifacts resulting from exclusion of fragments ejected at less than 1 km/s.

trary cutoff at 100,000 secondaries created a steep total SFD for relatively large secondary craters and a flatter SFD for the smaller secondaries. Soderblom et al. (1974) also used 100,000 secondaries per impact, but their plots do not extend to diameters smaller than ~500 m so the leveling off of the SFD is not shown. A steep SFD ($b > 4$) cannot be extrapolated over more than ~2 orders of magnitude in size without requiring greater mass than that excavated by the primary crater, so the slope must flatten at smaller sizes. Nevertheless, production of 10^7 or even 10^9 secondary craters does not violate reasonable constraints like the volume of solid material ejected at high velocity in a 10-km crater. Larger craters could produce much greater numbers of secondaries.

We approximate a curving SFD for secondaries based on our observations of Zunil and the results of our hydrodynamic simulation. We have measured b ranging from ~2 to 5 (Table 2) for small areas of rays, but these do not necessarily provide a good estimate of the total SFD of Zunil secondaries. However, we estimated a total of 10^7 craters $\geqslant$10 m and have not observed a Zunil secondary larger than 250 m, so using 250 m as the largest crater we must use $b = 5$ to produce 10^7 craters $\geqslant$10 m. This is steeper than the values of 3.5 to 4 reported for the secondaries of other craters by Shoemaker (1965) and Wilhelms et al. (1978), but also a smaller diameter for the largest secondary, as a fraction

Table 4
Models for the global average production of secondary craters

Reference, planet	SFD for large primary craters	D of largest primary	SFD for secondaries from a single impact	Ratio of largest secondary/primary	# Secondaries per impact	Crossover diameter, D_c
Shoemaker (1965), Moon	$b = 2$ (1–132 km)	132 km	$b = 4$ (or slightly less)	0.083 at 0.3 km 0.05 at 132 km	10^5	~200 m outside of rays
Soderblom et al. (1974), Mars	$b = 1$ (1–50 km)	50 km	$b = 3.5$	0.05	10^5	~1 km
This work, Mars	$b = 2$ (1–32 km) $b = 2.2$ (32–512 km)	Varies with geologic system (see Table 5)	$b = 5$ for 10^7 craters $b = 3$ for 10^7–10^8 craters	0.025	10^8	See Table 5

of the primary's diameter. The crater size distribution predicted from the hydrodynamic model (Fig. 14) has a much steeper slope for large secondaries, $b \sim 10$. However, there are probably many more large craters produced by clumps of fragments, especially close to the primary crater (Schultz and Gault, 1985; Vickery, 1986), so we use the observed $b = 5$ for $N \leqslant 10^7$ craters. We do use the hydrodynamic model to estimate the decrease in slope for smaller secondaries. Based on Fig. 14 we approximate the curvature with $b = 3$ for $N \leqslant 10^8$. Although primary craters larger than 10 km may produce more than 10^8 secondary craters, this has little effect on the total global SFD with $b \leqslant 3$.

For the production of large primary craters we prefer to use the best available martian observations rather than scaling from lunar production functions. For crater diameters from 1 to 32 km the SFD for young plains on Mars fits $b = 2$ (Barlow, 1988; data collected by R. Strom and published in Fig. 3d of Ivanov et al., 2002). The production of secondary craters is not very sensitive to the choice of production function from 1 to 32 km, except on very young terrains. For D larger than 32 km we used $b = 2.2$ after Hartmann (1999) for this model. However, the crossover diameter (D_c, the diameter below which secondaries outnumber primaries) is a strong function of the largest few primaries that contribute secondaries to a terrain under consideration, so the best way to estimate D_c would be to identify all of the possible contributing craters and use their actual sizes and ranges to the terrain.

In order to estimate the crossover diameter and the relative abundances of small primaries and secondaries, we also chose production functions for primaries smaller than 1 km. For D from 0.25 to 1 km we chose $b = 3.5$ based on measurements of Gaspra (Chapman et al., 1996). For primaries smaller than 250 m we chose $b = 2$ because we need a slope at least this flat in order to be minimally consistent with other evidence described in this paper.

The results of our modeling exercise are shown in two plots (Fig. 16), representing a largest primary of (a) 431 km (appropriate for the boundary between Early and Late Hesperian, i.e., the diameter of the largest crater likely to have formed, on average, at a time less than or equal to the age of this boundary) and (b) 108 km (appropriate for Middle to Late Amazonian). D_c correlates with size of the largest pri-

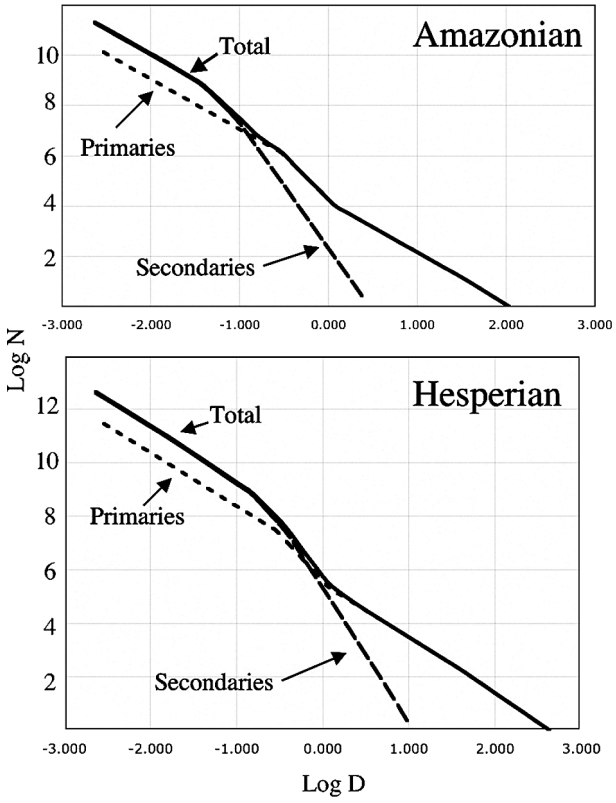

Fig. 16. Model SFD (see text) for primary craters, secondary craters, and the total. At top is a plot representative of terrains at the boundary between Middle and Upper Amazonian geologic time periods, and at bottom is a plot for the boundary between the Lower and Upper Hesperian. The crossover diameter (same number of primaries and secondaries) shifts to smaller diameters for younger terrains (see Table 5).

Table 5
Summary of global average crater SFD models

D_{max} (km)	Geologic system	D_c (m)	D where $Np = 10 \times Ns$
431	Early to Late Hesperian	600	1600 m
304	Hesperian to Amazonian	350	1200 m
215	Early to Middle Amazonian	210	840 m
152	Middle Amazonian	150	420 m
108	Middle to Late Amazonian	105	300 m
54	Late Amazonian	60	100 m

mary crater (Table 5). We also list (Table 5) the diameter at which primaries are ten times as abundant as secondaries, perhaps a safe minimum crater diameter to use for age estimates.

Table 5 shows global average results, but the density of secondary craters over a particular location will vary by 2 or more orders of magnitude depending on proximity to large primary craters younger than that surface. For example, with D_{max} of 9.5 km (~1 Ma terrain) the model predicts that primaries will dominate over secondaries at all sizes larger than 12 m. Secondaries larger than 12 m clearly dominate on the youngest surfaces within ~800 km of Zunil (10.1 km diameter). This model predicts that most of the craters resolved by MOC will be primaries on terrains younger than a few Ma, but the actual production function for small primaries is unknown. We also tried using $b = 4$ for secondaries ($N \leqslant 10^7$) and a largest secondary 5% as large as the primary, more in line with the values favored by previous workers, and this produced crossover diameters similar to those in Table 5.

4. Evidence that most small martian craters are secondaries

4.1. Morphology of small craters

From examination of many MOC images across Mars we have two qualitative impressions:

(1) small craters (typically 20–100 m diameter) are often clustered in space and especially in time (or age), and
(2) nearly all of the small craters appear shallow and flat-floored.

We present some measurements to verify the second impression.

Spatial clustering is best seen over young terrains where the small crater densities are well below saturation equilibrium. An example is shown in Fig. 17, in Chryse Planitia. Often the clustered craters are irregular and occur close to a plausible primary source crater. Spatial clustering is often not apparent in MOC images (typically only 3 km wide), yet most of the craters have the same state of degradation rather than a continuum from fresh and deep with sharp raised rims to very subdued depressions, as seen on the Moon. This uniformity could be explained by impacts that are clustered in time but spread out over large areas, as expected from distant secondaries. More quantitative studies are needed to verify these impressions of clustering in space and time.

The second impression is that nearly all of the small craters (less than ~500 m diameter) are shallow and flat-floored (e.g., Figs. 17–19): the shape and position of the crater interior shadows or shading in the few larger (>500 m) bowl-shaped craters (Figs. 17 and 18) differ from the shadows or shading in the many smaller craters. If eolian processes gradually fill in the small craters over time and the craters form by primary impacts with a range of ages, then there should be a continuum from bowl-shaped to infilled craters. Instead, small (<500 m diameter) craters that are actually bowl-shaped are very rare on Mars.

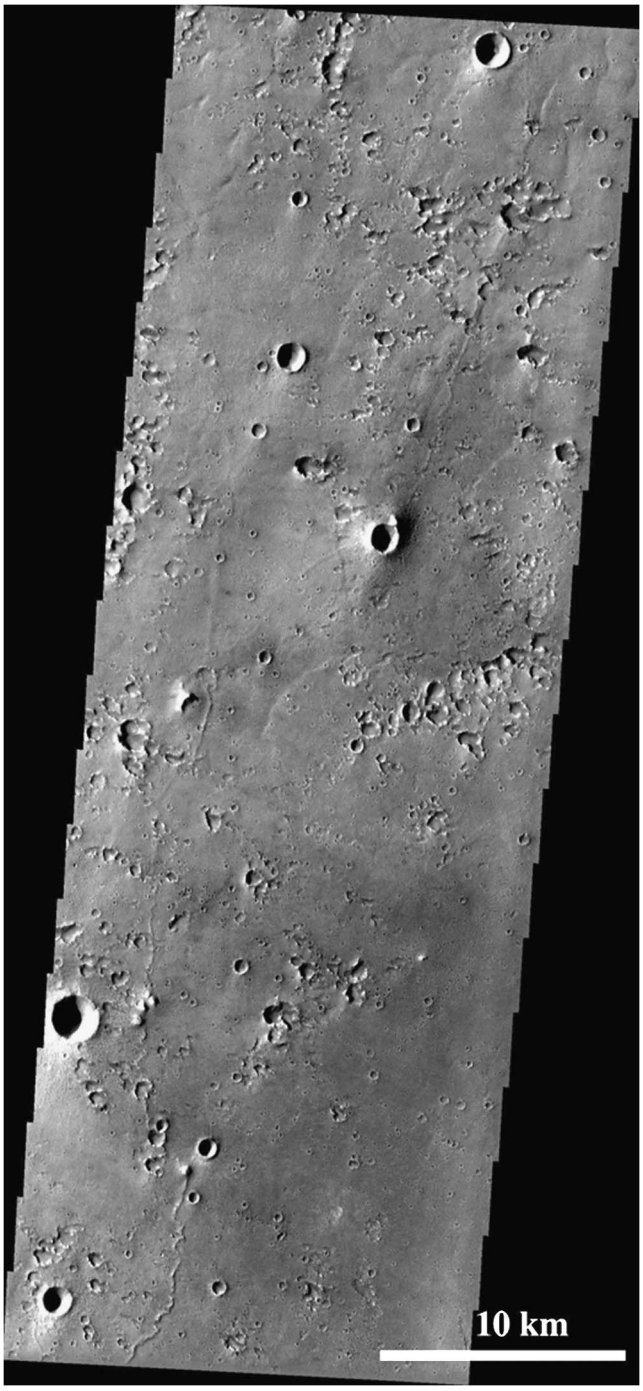

Fig. 17. THEMIS visible image V05369016 in Chryse Planitia (26° N, 323° W) showing clusters of irregular shallow craters, perhaps secondaries from a 30-km diameter crater at 26.5° N, 321.4° W. The circular bowl-shaped craters (6 are easily seen; the largest is 2 km diameter) are likely primaries. Swath width is 18 km, resolution is 18 m/pixel; Simple Cylindrical map projection.

Most small craters with sharp rims on Mars have different morphologies from small sharp-rimmed craters on the Moon, except for fresh lunar secondary craters. Pike

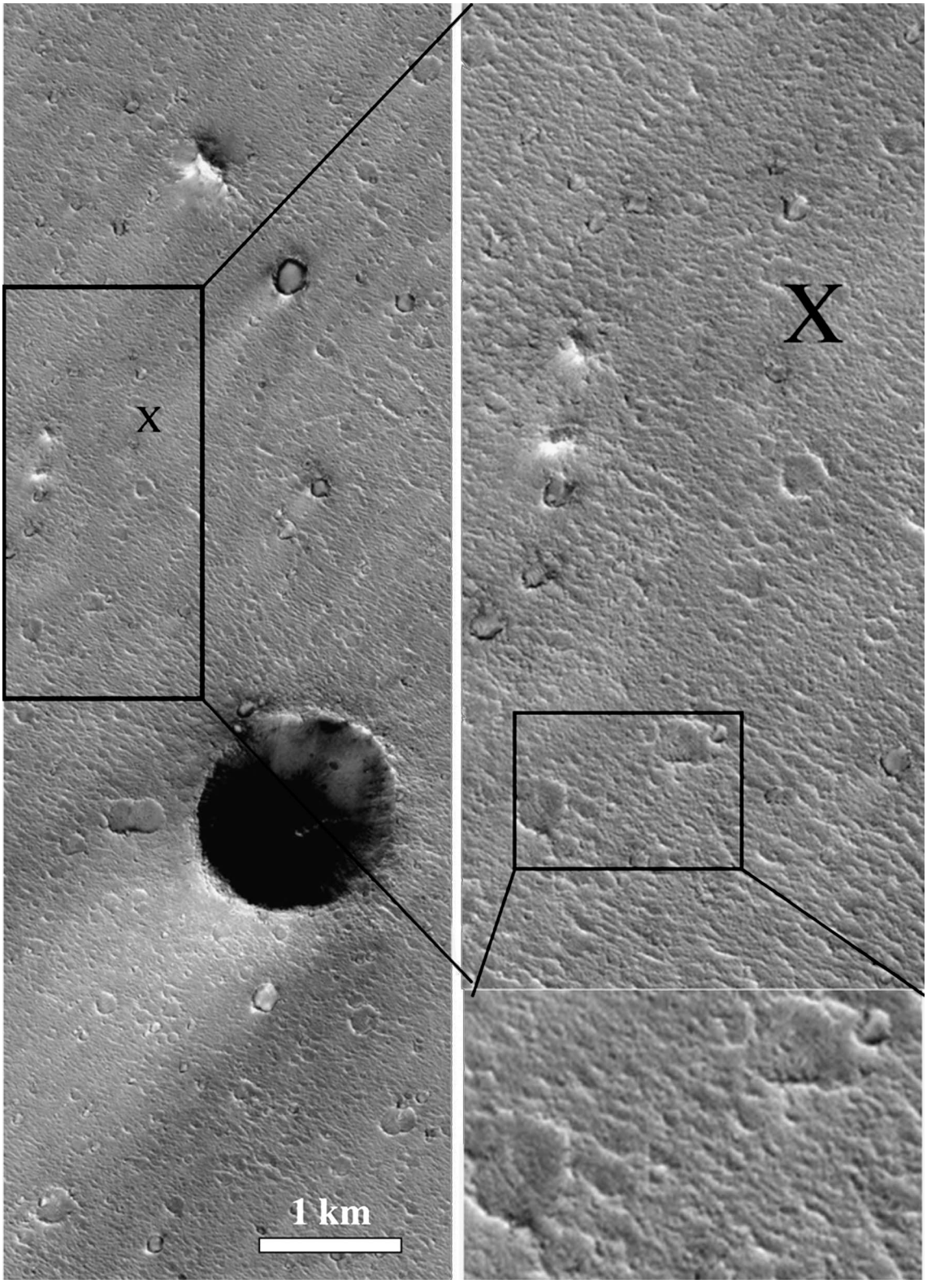

Fig. 18. Part of MOC image E12-01890 over the Mars Pathfinder landing site (marked by X). Scene is 3 km wide and scale is 1.8 m/pixel. "Big Crater" is the largest crater in the image. Part of the subscene is enlarged at right and again at bottom right to show finer details. Knobs to the lower left of the "X" are "Twin Peaks."

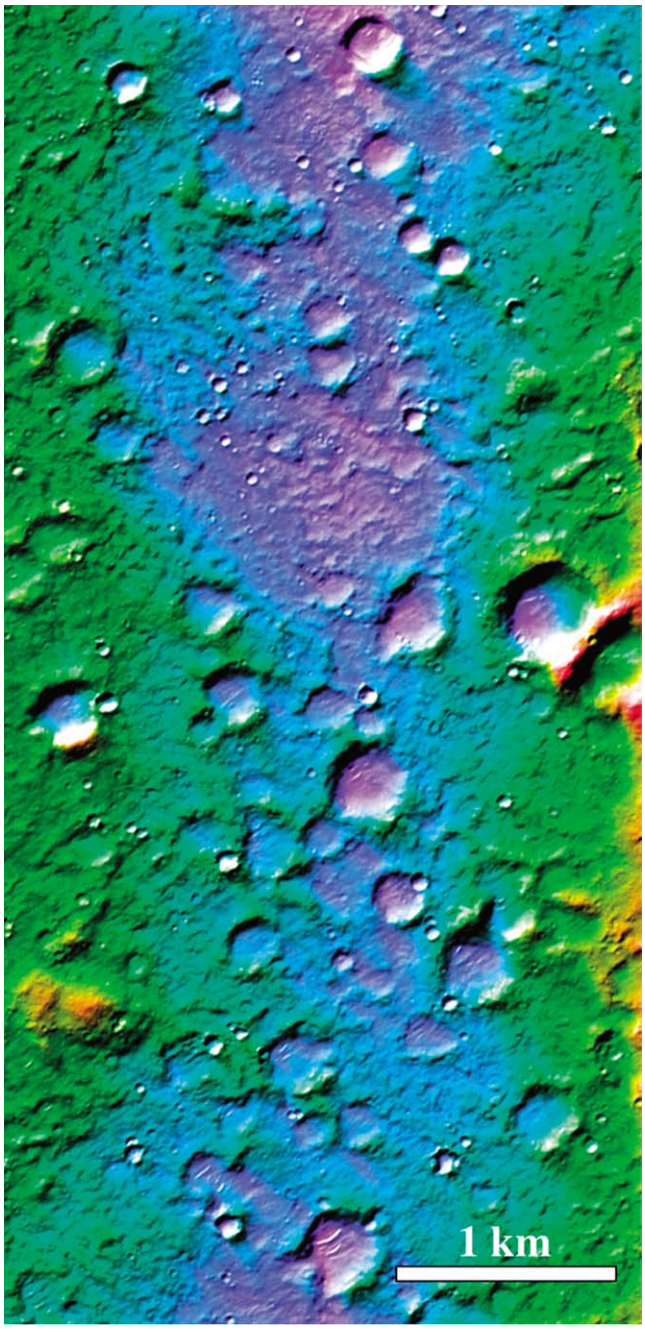

Fig. 19. A portion of a Digital Elevation Model in Gusev crater (Gusev 6), produced from MOC images E19-00218 and E21-00256 [see Table 1 and Fig. 29 of Kirk et al. (2003)]. Image is 3 km wide and the resolution is 3 m/pixel.

and Wilhelms (1978) carefully measured the shapes of 150 craters on the Moon that could confidently be identified as secondaries (from spatial distribution, clustering, and identification of the primary crater) with diameters of 43–200 m. They found the secondaries to be markedly less circular and to have shallower depth/diameter ratios and lower rim height versus diameter ratios, all of which are consistent with lower impact velocities, clustered impacts (Schultz and Gault, 1985), and oblique impact angles. Small craters commonly seen in narrow-angle MOC images are also shallower and less circular than fresh lunar craters and similar to the morphologies of very recent secondary craters from Zunil. For example, images of the Pathfinder landing region in Ares Vallis (Fig. 18) show surfaces with many small craters, but only "Big Crater" (~1.5 km diameter) has a bowl shape like a fresh primary crater on the lunar mare. All others appear to have much smaller depth/diameter ratios. If they were primary craters that are shallow due to eolian fill, then there must have been a very recent depositional event because few or no bowl-shaped craters have subsequently formed. Furthermore, the reduction of the crater's depth/diameter ratios by significant erosion and infilling after formation is not supported by estimates of erosion rates at the surface (Golombek and Bridges, 2000).

If all of the resolved small craters in the Ares Vallis region were primaries and the Hartmann–Neukum production function were used to estimate the abundance of even smaller craters, then this region should have experienced impact "gardening" to depths of 3–14 m (Hartmann et al., 2001). The presence of a regolith several meters thick is not consistent with the *Pathfinder* team's interpretation that the surface appears similar to what would have been expected soon after catastrophic floods ~3 Ga ago (Golombek et al., 1997; Smith et al., 1997). In particular, a series of troughs and ridges of 1–2 m amplitude, visible throughout the *Pathfinder* scene (Fig. 18), have been interpreted as ancient flood features (Golombek et al., 1999) and as younger transverse dunes (Greeley et al., 2000). MOC images of Tiu Valles (e.g., SP2-53005 and Fig. 8 of Malin and Edgett, 2001) show that the troughs and ridges are confined to channel floors and interrupted by the larger craters, supporting the fluvial interpretation. (The ridges are cut by craters in the Pathfinder region (Fig. 18) as well, so they must be older than the craters. This observation does not support the suggestion that the craters are shallow due to eolian infill.) We believe the ridges are ancient (Hesperian) fluvial features, but these 1–2 m high features could not be preserved if the surface had been uniformly gardened to depths of 3–14 m. Additional features of the Pathfinder site that could be difficult to explain if the surface had been gardened to several meters depth include tabular, subrounded rocks; imbricated boulders; boulder bars at the site that are similar to those deposited in catastrophic flood plains on the Earth; and the bands on south "Twin Peaks" interpreted as layering or downcutting episodes from the floods. Hertz et al. (1999) interpreted the rocks around Pathfinder to be impact ejecta rather than flood deposits, but the ridges and bands on "Twin Peaks" are nevertheless difficult to explain if the surface were gardened to several meters depth.

An alternative explanation is that the small craters seen in these regions are largely secondary craters. The shallow, flat-floored morphology would be close to the original form of these low-velocity (<5 km/s) impacts. Impact gardening still must have occurred, but to shallower depths and with less uniformity, perhaps allowing preservation of 2–3.5 Ga

old, meter-scale fluvial features in many areas. (See Section 4.3 for more in-depth discussion of regolith properties.)

Digital elevation models (DEMs) of MOC images were produced over portions of the candidate landing sites for MER to obtain quantitative information on topography and slopes for assessment of landing safety (Kirk et al., 2003; Golombek et al., 2003). Kirk et al. (2003) used digital stereogrammetry and two-dimensional photoclinometry (controlled by the stereogrammetry) to derive DEMs with 10 and 3 m spatial resolution, respectively. Crater dimensions were measured in two of the candidate landing sites, Gusev crater and Isidis Planitia, with multiple DEMs of cratered plains (Hurst et al., 2004). The surfaces should be considered as random samples of Hesperian (Isidis; Crumpler and Tanaka, 2003) and Late Hesperian/Early Amazonian (Gusev; Cabrol et al., 1998) surfaces. Both surfaces have a multitude of small craters comparable in number to those at the Pathfinder landing site. We measured the depth/diameter (d/D) ratios of 1300 craters in two 10-m DEMs of Isidis (95 craters in 65 km^2 in Isidis 1 and 58 craters in 15 km^2 in Isidis 2), five 10-m DEMs of Gusev (58 craters in 75 km^2 in Gusev 1, 26 craters in 56 km^2 in Gusev 2, 67 craters in 33 km^2 in Gusev 3, 68 craters in 44 km^2 in Gusev 4/5, and 105 craters in 36 km^2 in Gusev 6), one 6-m DEM of Gusev (195 craters in 5 km^2 in Gusev 3), and one 3-m DEM of Gusev (525 craters in 17 km^2 in Gusev 6), where the number refers to the DEM in Table 1 of Kirk et al. (2003). We also examined crater rim height versus diameter for the craters in the highest-resolution (3 m) DEM (Fig. 19), which is a portion of Gusev 6 in Kirk et al. (2003).

The best-fit d/D for all craters measured is 0.08 with a least-squares correlation coefficient of 0.8, slightly less than the 0.11 for the 150 secondaries measured by Pike and Wilhelms (1978) on the Moon and substantially less than the 0.2 d/D for primary craters on the Moon and Mars (Pike, 1977; Melosh, 1989). A summary of crater geometries from MOLA data (Garvin et al., 2003) reports $d = 0.21D^{0.81}$ for simple craters, which predicts d/D of 0.3 for 100-m-diameter primary craters. However, these estimates are extrapolations from measurements of larger craters, so we assume that 0.2 d/D is the best estimate for small primary craters on Mars. Examining the craters (10–475 m diameter) in the highest resolution DEM (3 m) in more detail showed that craters in different degradation states had different d/D ratios (Fig. 20). The freshest craters (class 1) with sharp rims and little evidence for modification have d/D of 0.11 with a least-squares correlation coefficient of 0.9. Class 2 craters with rounded rims and evidence for sediment deposited on their floors have d/D ratios of 0.045 with a least-squares fit of 0.9. Class 3 craters appear most degraded with muted low-relief rims, fairly flat floors and distinctly non-round planforms have d/D ratios of 0.03 with a correlation coefficient of 0.8. The fact that the freshest craters have values of d/D that match secondaries on the Moon argues that such craters are also secondaries on Mars. The observation that more degraded craters have even lower d/D suggests that

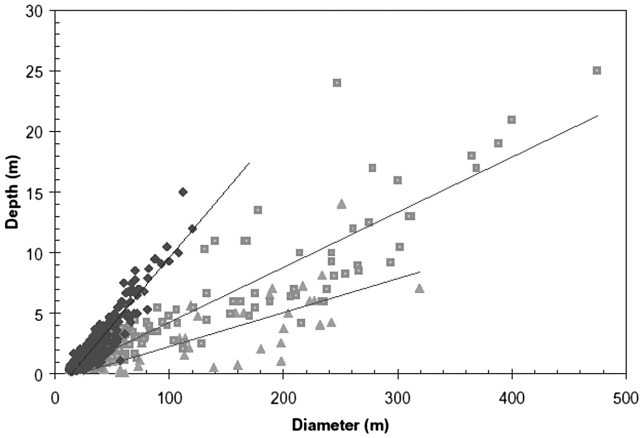

Fig. 20. Crater diameter versus depth plot of 3 classes of small craters in Late Hesperian/Early Amazonian plains within the Gusev crater landing ellipse of the MER Spirit, from the highest-resolution DEM, part of which is shown in Fig. 19. Craters were divided into 3 morphological classes. Class 1 craters have sharp rims and little evidence for degradation. Class 2 craters have more eroded, rounded rims, and flatter floors. Class 3 craters are the most degraded with muted rims. Diamonds are the d/D of 265 class 1 craters, which can be fit by a line of slope 0.11 with a correlation coefficient of 0.87. Squares are the 222 class 2 craters, which can be fit by a line of slope 0.045 with a correlation coefficient of 0.9. Triangles are the d/D of 38 class 3 craters, which can be fit by a line of slope 0.03 with a correlation coefficient of 0.8.

over geologic time the secondaries have been modified by erosion of their rims and deposition in their floors. Although it is possible that some of the craters (in all classes) are in fact degraded primary craters, the d/D values of the fresh craters (class 1) are inconsistent with fresh primary craters. The average rim height versus diameter ratio for the class 1 craters (0.0325) is intermediate between that measured for secondaries (0.02) and for primaries (0.04) (Pike and Wilhelms, 1978; Melosh, 1989). The SFD of the class 1 craters has a power-law slope (b) of 3.4, which is consistent with our modeling of the global average SFD of secondaries smaller than a few hundred meters on Hesperian terrains (lower plot in Fig. 16).

We have argued that widely separated samples of Hesperian cratered plains (Pathfinder, Gusev, and Isidis) are dominated by secondary craters at diameters smaller than ~250–500 m. The depth and rim height versus diameter ratios of small craters are both consistent with the lower impact velocities of rocks ejected from Mars rather than from the asteroid belt. We have also shown that sufficient numbers of secondaries could have been produced from the larger primary craters on Mars. If most small craters on the plains of Mars are in fact secondaries, there are important implications for the distribution of slopes and the roughness of such surfaces for future landed spacecraft (e.g., Gaskell, 1993; Bernard and Golombek, 2001).

The MER Spirit observations of Bonneville crater (Grant et al., 2004) provide an excellent example of a circular but shallow crater that is not infilled by eolian materials as often assumed (e.g., Hartmann, 1999). Bonneville crater (210 m diameter) has a depth/diameter ratio of only 0.07, yet it has

well-preserved primary morphologies and only a thin eolian infill, less than 1–2 m, so the MER science team concluded that it is a secondary crater. However, it certainly is not an "obvious" secondary crater in orbital images, and would not be excluded from crater counts for age dating.

4.2. Age of fine layered deposits

There are fine-layered deposits (FLDs) several km thick in many equatorial regions of Mars, perhaps originating from fluvial deposition, volcanic pyroclastics, eolian processes, or even polar processes (Malin and Edgett, 2000b, 2003; Ruff et al., 2001; Hynek et al., 2003; Schultz and Lutz, 1988). FLDs at the MER Opportunity region of Meridiani Planum have been interpreted as "dirty" evaporites, influenced by a combination of fluvial, eolian, and volcanic processes (Squyres et al., 2004; Klingelhofer et al., 2004). Multiple characteristics of the FLDs indicate that they are composed of fine-grained materials that are much more easily eroded by the wind than other geologic units. Many of the FLD surfaces are free of craters in MOC images, yet there are large embedded craters so these cannot be young deposits in many cases (Edgett and Malin, 2002). We consider the implications of few surface craters, particularly on mounds of FLD where eolian deposition is not likely to be hiding craters, using conservative assumptions (i.e., to make them as old as possible while assuming the NPF). A typical exposure imaged by MOC is $\sim$100 km^2 and a primary crater 16 m or larger should occur over this area every 15,000 years according to the NPF (which predicts fewer 16-m craters than the HPF). Let us assume an initial d/D of just 0.1 for high-velocity impact craters because these deposits are probably highly porous (Schultz, 2002; Housen, 2003). Erasing all craters 16 m in diameter (1.6 m deep) or larger requires an erosion rate of at least 100 m/Ma if the cratering were perfectly uniform over time. In fact, random processes like primary cratering are weakly clustered in time, so we cut this estimate in half to 50 m/Ma. At this rate a 10-km-thick deposit (to use a conservative upper limit on thickness) would be removed in just 190 Ma. However, the presence of interbedded impact craters up to 60 km in diameter requires much greater ages (Edgett and Malin, 2002). Malin and Edgett (2000b) interpreted the FLD as Late Noachian, but other workers suggest ages ranging from Late Noachian to Late Amazonian (summarized in Table 2 of Hynek et al., 2003). If we assume that some of the layers are 3 Ga old, then we have a factor of 16 discrepancy in our conservative example. One explanation could be that there has been a dramatic increase in erosion rates in just the past few Ma, but we suggest an alternative hypothesis.

What if most of the small craters on Mars are secondaries? If we only consider these to be low-velocity impacts (secondaries or decelerated primaries) and 60% as deep, then we can cut the erosion rate by 40%, a small change. However, secondary craters are highly clustered in space and time. Instead of assuming random primary cratering with two craters $\geqslant$16 m per 30,000 years over a 100-km^2 area, we assume that 50 craters $\geqslant$16 m form simultaneously every 450,000 years on average. The average timescale for formation of a 10-km crater like Zunil is $\sim$1 Ma, which forms secondary craters $\geqslant$16 m over an area covering $\sim$5% of Mars, so any region of Mars might experience a secondary crater shower every $\sim$20 Ma. All primary craters smaller than Zunil expected within 1 Ga make a similar contribution to secondary craters $\geqslant$16 m, so 10 Ma may be about the right frequency for secondary showers, but there must also be small primary craters; we use 0.45 Ma for this conservative example. (If we assumed cratering in rays like those of Zunil, the estimate would be $\sim 10^3$ craters every 9 Ma, but the example we use here may be more appropriate for the very distant secondaries where rays are not recognizable.) Combining this with our previous assumptions (and d/D of 0.1), we need an erosion rate of just 2.1 m/Ma to explain the lack of craters, so a 10-km stack of FLD could survive 4.7 Ga. We should also expect to see some FLDs peppered with small craters, as observed (e.g., E11-02725 in west Candor Chasma). Superpositions indicate that many layered deposits are younger than Noachian (Hynek et al., 2003, and references therein), but the absence of small craters does not rule out the hypothesis that some FLDs date back to the Noachian. An erosion rate of order 1 m/Ma is five orders of magnitude higher than the $\sim 10^{-5}$ m/Ma post-Noachian erosion rate estimated by Golombek and Bridges (2000), but clearly the FLDs are eroding much faster than other terrains on Mars.

4.3. Regolith thicknesses

Hartmann et al. (2001) applied an average of the Hartmann and Neukum production functions to estimate regolith production from impact "gardening" as a function of terrain age. They show that Late Hesperian/Early Amazonian terrains such as the Pathfinder and the two Viking landing sites have crater densities from 0.1 to 1.0 times that of the lunar maria, and conclude that these terrains should have experienced cumulative gardening of 3–14 m. This conclusion conflicts with the interpretations of the science teams for the Viking Landers (Binder et al., 1977; Mutch et al., 1977) and Pathfinder (Golombek et al., 1997; Smith et al., 1997; discussed above in Section 3.1). We suggest two variations on the analysis of Hartmann et al.: (1) most of the small craters may be shallow due to low-velocity secondary impacts, gardening to about 60% the depth of high-velocity primaries; and (2) there may be fewer impact craters than estimated by Hartmann et al. at diameters smaller than those actually counted. The crater counts of Hartmann et al. (2001) extend down to diameters of $\sim$60 m on the VL1 and Pathfinder terrains, but most of the gardening is accomplished by the more numerous craters smaller than 20 m in diameter. The number of craters smaller than 60 m was estimated via extrapolation of the assumed production function; extrapolation from 60 m leads to the lower

limit of 3 m regolith. However, very few published SFDs for Mars actually follow the HPF (e.g., Figs. 2, 5–9 of Hartmann et al., 2001). Instead, the SFDs for small craters are flatter, i.e. crater counts almost all fall on younger HPF isochrons for smaller craters. For estimation of regolith depths it does not matter how this falloff is explained (e.g., the presence of thin younger units on the surface or a shallower production function). Based on the actual trends shown by the published SFD plots, we should expect the number of 10-m-diameter craters to be ∼5 times less than the extrapolation of the averaged HPF-NPF from 60-m-diameter craters. Applying this modification and the 40% reduction in gardening by low-velocity impacts, we estimate that the average regolith depth on the landing sites is ∼0.4 m. Also, if dominated by secondary cratering, regolith thickness will be spatially variable (perhaps ranging from 0 to 1 m) due to the clustering of secondary impacts. The presence of a thin regolith of variable thickness is more consistent with the observations at the three landing sites and with the fact that Late Hesperian and Early Amazonian terrains, imaged by MOC at 1.5–3 m/pixel, do not appear to be topographically smoothed by a mantle of regolith, as do the lunar maria imaged at the same scale.

4.4. Consistency of age constraints from small and large craters

It is difficult to reconcile the HPF and NPF with the small-crater age constraints imposed by the existence of at least three young craters larger than 10 km in diameter on Mars. All three craters appear to be very young on the basis of the sparse densities of small craters superimposed either on the large-crater deposits or surfaces older than the large-crater deposits. These craters are (1) Zunil (7.7° N, 166° E), (2) McMurdo (84° S, 0° E), and (3) an unnamed crater just west of the Olympus Mons aureole (23° N, 207° E).

(1) There are no detectable impact craters on the interior or continuous ejecta blanket of Zunil imaged by MOC, ∼600 km^2 area. A crater ⩾24 m diameter (easily resolved in 3 m/pixel MOC images) should occur every 2 or 8 Ka over this 600 km^2 area according to the HPF and NPF, respectively, so Zunil should be younger than ∼10 Ka. However, we expect a crater ⩾10 km in diameter to be formed about every 1 Ma somewhere on Mars (Ivanov, 2001), and we may be able to detect large rayed craters over only ∼20% of Mars (discussed in Section 2.1), so Zunil is most likely ∼5 Ma from this large-crater constraint. Of course it could be much younger than 5 Ma, but the chances that is younger than 10 Ka is less than 0.002 so this is highly unlikely.
(2) An even more unlikely scenario is required to explain the paucity of small primary craters on the south-polar layered deposits, given the superposition of the 23-km-diameter McMurdo crater and its field of secondary craters. A McMurdo-sized crater is expected on an area the size of the south-polar layered deposits every 90–180 Ma, but explaining the lack of primary craters on the layered deposits requires that the McMurdo impact happened within the past 100 Ka according to Schaller et al. (2003). The probability of this occurrence is ∼0.001.
(3) A 29-km-diameter crater just west of the Olympus Mons aureole appears pristine and has few or no superposed impact craters (Mouginis-Mark et al., 2003). Furthermore, Mouginis-Mark et al. (2003) report no impact craters resolvable at 6 m/pixel (craters ∼24 m in diameter or larger) over a 72-km^2 ejecta lobe. We should expect a crater ⩾24 m over an area of this size every 17 Ka according to the HPF, or every 68 Ka according to the NPF. However, a crater 29 km or larger forms somewhere on Mars only every ∼5 Ma via either HPF or NPF. If this is the very youngest crater ⩾29 km on Mars, then the probability that it as young as 68 Ka is less than 0.014.

All three of these craters are superimposed on Late Amazonian terrains [covering just 7% of Mars, Tanaka (1986)]. This is probably not a coincidence: fresh craters are easier to recognize on young terrains and have been imaged at high resolution more often than craters of comparable size on older terrains. According to the HPF or NPF we should expect 2 craters ⩾20 km to be created on 7% of Mars in ∼70 Ma. However, the paucity of small craters postdating these impacts indicates ages of less than 100 Ka, at least a 700-fold disparity with the NPF; >2000 with the HPF. Either Mars has experienced two highly improbable impacts in the last 100 Ka (plus another one—Zunil—in the last 10 Ka), or the HPF and NPF predict too many small primary craters.

Given other evidence presented in this paper that secondaries are more abundant than primaries for small craters (<250 m), we conclude that the HPF and NPF must predict too many small primary craters. Our global average cratering model (Section 3.2) predicts numbers of small (∼26 m) secondary craters comparable to the numbers predicted by the NPF. We need to reduce the production of small primary craters by ∼10^3 compared with the NPF and HPF to bring it into line with the observations at these three large primary craters. In Section 3.2 we choose a conservative reduction of small primary craters, ∼10 times less than predicted by the NPF at 26 m (the typical diameter of small craters resolved by MOC).

An additional piece of evidence that the Hartmann chronology based on small craters is incorrect comes from the work of Quantin et al. (2004), who measured the crater ages of 66 landslide deposits in Valles Marineris with the HPF. Their Fig. 13, number of landslides versus time, shows the frequency of landslides increasing exponentially to the present, as if the slopes of Valles Marineris are becoming increasingly unstable. (The younger landslides do not appear to be completely obscuring older landslide deposits.) Decreasing the slope of the production function for small craters would produce a more constant rate of landslide for-

mation over time, although the effects of secondary craters also enlarge the error bars.

5. Further discussion

5.1. Implications for age constraints on young surfaces

Concerns about the origins and modification of small craters has led some investigators to avoid using craters smaller than ∼1 km for age constraints (e.g., Strom et al., 1992; Plescia, 2003). However, there are very few if any craters larger than 1 km on the youngest martian terrains, which are of great interest for the study of recent geologic activity or climate change, and we currently have no other way of estimating ages unless rates of change can be directly observed. Our modeling results confirm that the diameter at which secondaries dominate (D_c) becomes smaller for younger terrains, so potentially we can date younger terrains (age constrained to first order by craters >1 or 2 km) using craters smaller than 1 km, if a large and younger primary crater is not identified within a few hundred km. Table 5 gives D_c as a function of the largest primary crater contributing secondaries (D_{max}), which corresponds approximately to the time-stratigraphic units of Tanaka (1986). We also give the diameters at which primaries are ten times as abundant as secondaries, which provides a reasonable "safe" limit for dating surfaces. These numbers suggest that we could rely on craters smaller than 300 m on Late Amazonian terrains, but we have presented evidence that the production function for primary craters is poorly known below a diameter of ∼300 m. (How well the production function is really known at larger diameters is a matter of continuing debate, but the published models generally agree to within a factor of 2 to 3.) Pending further work, we recommend the following minimum crater diameters for age constraints: 1600 and 1200 m for the Early and Late Hesperian, respectively; 840, 420, and 300 m for the Early, Middle, and Late Amazonian, respectively.

Given these guidelines, what is the maximum age we can assign to terrains free of any craters larger than 300 m? We expect the number of primary craters $\geqslant$300 m/km^2/Ma to be $\sim 3.5 \times 10^{-5}$ via both NPF and HPF over the past 3.4 Ga (Ivanov, 2001). The production function we use in Section 3.2 is within a factor of two of this value. Therefore, the maximum cratering age is a function of the area of a crater-free unit (i.e., terrain that is thought to have been shaped by the same process and period of time). For terrains covering $\sim 10^2$ km^2, like sets of gullies and debris aprons within a large crater, the upper age limit is ∼300 Ma, greater than the few Ma upper limit suggested by Malin and Edgett (2000b). Mustard et al. (2001) stated that the absence of craters larger than 100 m on the mid-latitude debris mantle indicates a maximum age of 0.15 Ma via the HPF. Recalculating for the absence of craters larger than 300 m with the HPF increases the maximum age to 10 Ma. If we assume $b = 3$ for craters from 0.3–1 km diameter, then the maximum age increases to ∼30 Ma. Since many gullies cut this debris mantle, their age limit is also ∼10 to 30 Ma. There has been recent activity and climate change on Mars, but we cannot justify correlations with very recent (order 10^5 yr) obliquity cycles (Head et al., 2003) given our current state of understanding.

5.2. Age of Athabasca Valles

Athabasca Valles (AV) may mark the most recent catastrophic flooding (peak discharge $>10^6$ m^3/s; Burr et al., 2002b), so its absolute age is important to understanding the history of water on Mars. There has been some confusion over the chronology of events in AV. Plescia (1990, 2003) used statistics of craters with diameters >1 km to bracket the age of the last Athabasca channel outflow event to between 1.7 Ga (ridged plains) and 144 Ma [young lavas in western Cerberus plains (WCP)]. However, most craters larger than 500 m diameter in the WCP are embayed by young lavas, and some apparently young lavas are in turn cut by AV (Lanagan and McEwen, 2003). Based on the HPF and counts of small craters (<200 m) on the floor of Athabasca Valles, Burr et al. (2002a) estimated the age of the last Athabascan fluvial event to be from 2–8 Ma. Some of the floor of AV is covered by lava flows, which must be younger than the aqueous flooding, but much of the channel area is not covered by flows and Lanagan et al. (2001) and Burr et al. (2002a, 2002b) argued that the volcanism must have quickly followed the flooding, because rootless cones are observed. We now realize that ∼80% of the craters superimposed on the channel floors are secondary craters from Zunil, and suggest that a more credible constraint is the absence of craters larger than ∼300 m. The area of channel floor imaged by MOC at better than 6 m/pixel is about 300 km^2, consistent with a maximum age of ∼200 Ma. Werner et al. (2003) applied crater counts to the NPF and concluded that major fluvial processes ended 2.6 Ga ago but with volcanic activity extending to as recently as 3 Ma. However, they (1) incorrectly assumed that the flooding could be no younger than the terrain it cuts; (2) neglected the higher, grooved portions of channel floor that do not appear to be covered by lavas (Keszthelyi et al., 2004a); and (3) neglected patches of sparsely cratered lava cut by AV (Lanagan and McEwen, 2003).

Based on observations of Athabascan channels that cut through pristine lava surfaces and are also embayed by other lava surfaces, Lanagan and McEwen (2003) argue that Athabascan fluvial outflows were contemporaneous with the emplacement of many WCP lavas. Additionally, they note that an analysis of high-resolution (2–20 m/pixel) images of the WCP shows that lava flows embay or fill all but one 500-m impact crater imaged by MOC, suggesting that the WCP should be no older than 100 Ma, or perhaps 200 Ma with a factor of two uncertainty (e.g., Hartmann, 1999). Clearly the channel formed before the Zunil impact event,

which is ∼1.5 or 2.7 Ma if it was the source of some of the basaltic shergottites (Section 2.4). In summary, we estimate that the Athabascan flooding occurred between 1.5 and 200 Ma ago.

5.3. Why are there fewer small primary craters than expected?

We have described evidence for a flattening of the production function for primary craters smaller than ∼300 m on Mars compared with the NPF and HPF, and for a secondary origin for most of the small craters. This result is surprising because previous workers have concluded that Mars and the Moon are cratered by the same population of small bodies from the asteroid belt (reviewed by Ivanov et al., 2002). We consider a number of explanations. Perhaps eolian processes on Mars erase primary craters faster than secondaries, but we have not been able to posit a reasonable scenario where this would be true. This leaves two other possibilities, described below.

The first hypothesis is that the long-term average atmospheric density of Mars has significantly reduced the production of small primary craters, and to a greater extent than it reduced the production of small secondary craters. Aerodynamic stresses are roughly proportional to velocity squared (Melosh, 1989), so a body entering the atmosphere at 10 km/s (typical for asteroid fragments at Mars) will experience ∼10 times the stress level of a body entering at 3 km/s (typical for a distant secondary crater). Once fragmented, the smaller bodies are more efficiently decelerated and ablated. Chappelow and Sharpton (2003) analyzed these effects and projectile properties, and found that the current 6.1 mbar atmosphere reduces the production of 26-m-diameter primary craters by a factor of ∼5. (Craters abundant on MOC images are typically ∼26 m diameter.) We think a reduction of at least a factor of 100 better explains the observations (Section 4.4). Reduction by a factor of 30 is possible with a 50-mbar atmosphere according to Chappelow and Sharpton (2003). However, if atmospheric density is controlled by changes in obliquity (Kieffer and Zent, 1992), then the small crater record will be dominated by cratering during the times of low obliquity and insignificant atmospheric pressure. Consider a simple example in which the atmosphere has no effect on the formation of 26-m craters for 50% of the time and completely eliminates 26-m craters 50% of the time. The density of 26-m craters will be reduced by only a factor of two. To reduce the number of ∼26-m-diameter craters by a factor of 100 requires that Mars have a climate history that very rarely allows the atmospheric pressure to be as low as that of today, a scenario that has not been proposed.

We are left with the conclusion that the production function for lunar craters smaller than 300 m has not been correctly estimated and/or is dominated by secondary craters. Since the lunar maria reach saturation equilibrium below ∼250 m diameter, estimation of the NPF has been based on counts of small craters superimposed on the deposits of young Copernican craters (Neukum et al., 1975, 2001), but these could be mostly distant secondary craters. In this case the flattening of the SFD reflects the actual population of small asteroidal fragments crossing the orbits of Mars and Earth. This hypothesis has gained support from the recent theoretical modeling and data analysis of Bottke et al. (2005), in which they conclude that the production function for craters smaller than ∼1 km should have cumulative slope, b of ∼3.

6. Summary and conclusions

6.1. Zunil

- A system of rays, composed of dense concentrations of secondary craters, are mapped around the 10-km crater named Zunil in the Cerberus plains, and extend as far as 1600 km from the crater.
- Zunil created $\sim 10^7$ secondary craters from 10 to 100 m diameter.
- There are few secondary craters within ∼16 crater radii; they were almost all formed at greater ranges. There are almost none of the “obvious secondary craters” that are routinely excluded from crater counts for age dating.
- Zunil is a plausible source crater for some of the basaltic shergottites with emplacement ages of 165–177 Ma and ejection ages of either ∼1.5 or ∼2.7 Ma.
- A simulation of a Zunil-like impact ejected $\sim 10^9$ rock fragments capable of forming distant secondary craters $\geqslant$10 m; many rocks would escape Mars and could become Martian meteorites found on Earth.
- According to the simulation, ∼70% of the craters larger than 10 m in diameter form at distances of 800 to 3500 km, whereas most craters larger than 50 m form within 800 km of the primary.

6.2. Most small martian craters may be secondaries

- If Zunil were close to typical, most small craters on Mars could be distant secondaries.
- If Zunil produced an unusually large number of secondaries, most small craters on Mars could nevertheless be secondaries if the production of small primary craters is significantly less than predicted by the NPF.
- Most small craters near the Pathfinder landing site appear to be secondaries.
- Measurements of 1300 small craters over Gusev crater and Isidis Planitia show that they have depth/diameter ratios of ∼0.11 or less, consistent with lunar secondary craters and much shallower than expected for primaries.
- The fine-layered deposits on Mars can be billions of years old yet erode fast enough to remove almost all small craters if the cratering is strongly clustered in time from secondary cratering.

6.3. Mars has fewer small primary craters than predicted by the HPF and NPF

- The regolith thicknesses at past landing sites appear to be far less than predictions from the Hartmann/Neukum production functions, suggesting that craters smaller than 60 m form less often than predicted by these functions.
- Age estimates on three large (10, 23, and 29 km) craters based on Hartmann/Neukum production functions for small craters suggest highly improbable events in the last 10–100 Ka. Alternatively, the production functions predict too many small primary craters.
- Atmospheric filtering or eolian processes cannot adequately explain the numbers of small primary craters, so these numbers probably reflects the size distribution of small bodies ejected from the asteroid belt that crossed the orbits of Mars and Earth.

6.4. Age constraints from small craters

- The crossover diameter, below which secondaries are more abundant (globally) than primaries, shifts to smaller diameters for younger terrains, so it is possible to choose "safe" minimum crater diameters for age dating.
- We do not understand the production function for primary craters smaller than ∼1 km and especially below ∼300 m on Mars, except that it must be "flatter" than previously assumed below ∼300 m.
- The absence of craters larger than 300 m in diameter on the mid-latitude debris mantle gives a maximum age of 10 Ma or more, which is too coarse to correlate with obliquity cycles.
- Water release from Athabasca Valles, perhaps the most recent catastrophic flooding on Mars, occurred between 1.5 and 200 Ma ago.

Acknowledgments

We thank many colleagues for discussions and communications related to this research, including Joe Boyce (Univ. Hawaii at Manoa), Clark Chapman and Bill Bottke (SWRI, Boulder), Bill Hartmann and Betty Pierazzo (PSI, Tucson), Jim Head (Raytheon Corp., Tucson), Laszlo Keszthelyi and Ken Tanaka (USGS, Flagstaff), Mike Malin and Ken Edgett (MSSS, San Diego), and Jay Melosh and Bob Strom (Univ. Arizona). We thank Jennifer Blue (USGS, Flagstaff) for facilitating IAU approval of the name "Zunil," and Trent Hare (USGS, Flagstaff) for help accessing and interpreting the Mars Crater Database (http://webgis.wr.usgs.gov). This research supported by the Mars Data Analysis Program and Mars Odyssey THEMIS.

References

Artemieva, N.A., Ivanov, B.A., 2004. Launch of martian meteorites in oblique impacts. Icarus 171, 84–101.
Artemieva, N.A., Pierazzo, E., 2003. Oblique Impact and it's ejecta: Numerical modeling. Impact cratering: Bridging the gap between modeling and observations. LPI Contribution 1155, 10–11.
Asphaug, E., Melosh, H.J., 1993. The Stickney impact of Phobos: A dynamical model. Icarus 101, 144–164.
Baker, V.R., 2001. Water and the martian landscape. Nature 412, 228–236.
Bandfield, J.L., Hamilton, V.E., Christensen, P.R., 2000. A global view of martian volcanic compositions. Science 287, 1626–1630.
Barlow, N.G., 1988. Crater size–frequency distributions and a revised martian relative chronology. Icarus 75, 285–305.
Barlow, N.G., 2003. Utilizing diverse data sets in martian impact crater studies. Sixth International Conference on Mars. Abstract 3072.
Berman, D.C., Hartmann, W.K., 2002. Recent fluvial, volcanic, and tectonic activity on the Cerberus plains of Mars. Icarus 159, 1–17.
Bernard, D.E., Golombek, M.P., 2001. Crater and rock hazard modeling for Mars landing. American Institute of Aeronautics and Astronautics, Space 2001 Conference, Albuquerque, NM, August 2001, Paper AIAA-2001-4697, CD-ROM, 17 pp.
Bierhaus, E.B., Chapman, C.R., Merline, W.J., Brooks, S.M., Asphaug, E., 2001. Pwyll secondaries and other small craters on Europa. Icarus 153, 264–276.
Binder, A.B., Arvidson, R.E., Guinness, E.A., Jones, K.L., Mutch, T.A., Morris, E.C., Pieri, D., Sagan, C., 1977. The geology of the Viking Lander 1 site. J. Geophys. Res. 82, 4439–4451.
Bottke, W.F., Durda, D.D., Nesvorny, D., Jedicke, R., Morbidelli, A., Vokrouhlicky, D., Levison, H., 2005. Icarus. Submitted for publication.
Bottke, W.F., Nesvorny, D., Durda, D.D., 2005. Are most small craters primaries or secondaries: Insights from asteroid collisional/dynamical evolution models. Lunar Planet. Sci. XXXVI. Abstract 1489.
Brown, P., Spalding, R.E., ReVelle, D.O., Tagliaferri, E., Worden, S.P., 2002. The flux of small near-Earth objects colliding with the Earth. Nature 420, 294–296.
Burr, D.M., Grier, J.A., Keszthelyi, L.P., McEwen, A.S., 2002a. Repeated aqueous flooding from the Cerberus Fossae: Evidence for very recently extant, deep groundwater on Mars. Icarus 159, 53–73.
Burr, D.M., McEwen, A.S., Sakimoto, S.E.H., 2002b. Recent aqueous floods from the Cerberus Fossae, Mars. J. Geophys. Res. Lett. 29, 10.1029/2001GL013345.
Cabrol, N.A., Grin, E.A., Landheim, R., Kuzmin, O., Greeley, R., 1998. Duration of the Ma'adim Vallis/Gusev crater hydrologic system. Icarus 133, 98–108.
Carr, M.H., 2001. Mars Global Surveyor observations of martian fretted terrain. J. Geophys. Res. 106 (E10), 23,571–23,954.
Chapman, C.R., Haefner, R.R., 1967. A critique of methods for analysis of the diameter–frequency relation for craters with special application to the Moon. J. Geophys. Res. 72, 549–557.
Chapman, C.R., Veverka, J., Belton, M.J.S., Neukum, G., Morrison, D., 1996. Cratering on Gaspra. Icarus 120, 231–245.
Chappelow, J.E., Sharpton, V.L., 2003. Atmospheric effects and the record of small craters on Mars. Lunar Planet. Sci. XXXIV. Abstract 1418.
Christensen, P.R., 2003. Formation of recent martian gullies through melting of extensive water-rich snow deposits. Nature 422, 45–48.
Christensen, P.R., 21 colleagues, 2003. Morphology and composition of the surface of Mars: Mars Odyssey THEMIS results. Science 300, 2056–2061.
Christensen, P.R., 13 colleagues, 2005. Mars Exploration Rover candidate landing sites as viewed by THEMIS. Icarus. In press.
Crumpler, L., Tanaka, K., 2003. Geology and MER target site characteristics along the southern rim of Isidis Planitia, Mars. J. Geophys. Res. 108 (E12), 8080.
Edgett, K.S., Malin, M.C., 2002. Martian sedimentary rock stratigraphy: Outcrops and interbedded craters of northwest Sinus Meridiani and southwest Arabia Terra. Geophys. Res. Lett. 29, 2179.

Garvin, J.P., Sakimoto, S.E.H., Frawley, J.J., 2003. Craters on Mars: Global geometric properties from gridded MOLA topography. Sixth International Conference on Mars. Abstract 3277.

Gaskell, R.W., 1993. Martian surface simulations. J. Geophys. 98, 11,099–11,103.

Gault, D.E., Wedekind, J.A., 1978. Experimental studies of oblique impact. Lunar Planet. Sci. IX, 3843–3875.

Golombek, M.P., Bridges, N.T., 2000. Erosion rates on Mars and implications for climate change: Constraints from the Pathfinder landing site. J. Geophys. Res. 105, 1841–1853.

Golombek, M.P., 13 colleagues, 1997. Overview of the Mars Pathfinder mission and assessment of landing site predictions. Science 278, 1743–1748.

Golombek, M.P., 14 colleagues, 1999. Overview of the Mars Pathfinder Mission: Launch through landing, surface operations, data sets, and science results. J. Geophys. Res. 104, 8523–8554.

Golombek, M.P., 21 colleagues, 2003. Selection of the Mars Exploration Rover landing sites. J. Geophys. Res. 108, 8072.

Grady, E.E., Kipp, M.E., 1980. Continuum modeling of explosive fracture in oil shale. Int. J. Rock Mech. Min. 17, 147–157.

Grant, J., 22 colleagues, 2004. Surficial deposits at Gusev crater along Spirit rover traverses. Science 305, 807–810.

Greeley, R., Iverson, J., 1985. Wind as a Geological Process. Cambridge Univ. Press, New York.

Greeley, R., Kraft, M.D., Kuzmin, R.O., Bridges, N.T., 2000. Mars Pathfinder landing site: Evidence for a change in wind regime and climate from lander and orbiter data. J. Geophys. Res. 105, 1829–1840.

Grier, J.A., Hartmann, W.K., 2000. Rayed craters as probes of the upper surface of Ma'adim Vallis and Elysium Planitia: Images from Mars Global Surveyor. Lunar Planet. Sci. XXXI. Abstract 1478.

Hartmann, W.K., 1969. Lunar and interplanetary rock fragmentation. Icarus 10, 201–213.

Hartmann, W.K., 1999. Martian cratering. VI. Crater count isochrons and evidence for recent volcanism from Mars Global Surveyor. Meteorit. Planet. Sci. 34, 167–177.

Hartmann, W.K., 10 colleagues, 1981. Chronology of planetary volcanism by comparative studies of planetary cratering. In: Basaltic Volcanism on the Terrestrial Planets, pp. 1049–1127.

Hartmann, W.K., Gaskell, R.W., 1997. Planetary cratering. 2. Studies of saturation equilibrium. Meteorit. Planet. Sci. 32, 109–121.

Hartmann, W.K., Berman, D.C., 2000. Elysium Planitia lava flows: Crater count chronology and geological implications. J. Geophys. Res. 105, 15,011–15,026.

Hartmann, W., Neukum, G., 2001. Cratering chronology and the evolution of Mars. Space Sci. Rev. 96, 165–194.

Hartmann, W.K., Anguita, J., de la Casa, M., Berman, D., Ryan, E.V., 2001. Martian cratering. 7. The role of impact gardening. Icarus 149, 37–53.

Head, J.N., Melosh, H.J., Ivanov, B.A., 2002. Martian meteorite launch: High-speed ejecta from small craters. Science 298, 1752–1756.

Head, J.W., Mustard, J.F., Milliken, M.A., Ralph, E., Marchant, D.R., 2003. Recent ice ages on Mars. Nature 426, 797–802.

Hertz, F., Cintala, M.J., Rochelle, W.C., Kirk, B., 1999. Collisionally processed rocks on Mars. Science 285, 2105–2107.

Housen, K.R., 2003. Material motions and ejection velocities for impacts in porous targets. Lunar Planet. Sci. XXXIV. Abstract 1300.

Housen, K.R., Schmidt, R.M., Holsapple, K.A., 1983. Crater ejecta scaling laws: Fundamental forms based on dimensional analysis. J. Geophys. Res. 88, 2485–2499.

Hurst, M., Golombek, M.P., Kirk, R., 2004. Small crater morphology within Gusev crater and Isidis Planitia: Evidence for widespread secondaries on Mars. Lunar Planet. Sci. XXXV. Abstract 2068.

Hynek, B.M., Phillips, R.J., Arvidson, R.E., 2003. Explosive volcanism in the Tharsis region: Global evidence in the martian geologic record. J. Geophys. Res. 108 (E9), 5111.

Ivanov, B.A., 2001. Mars/Moon cratering ratio estimates. Space Sci. Rev. 96, 87–104.

Ivanov, B.A., Neukum, G., Bottke, W.F., Hartmann, W.K., 2002. The comparison of size–frequency distributions of impact craters and asteroids and the planetary cratering rate. In: Bottke, W.F., Cellino, A., Paolicchi, P., Binzel, R.P. (Eds.), Asteroids III. Univ. of Arizona Press, Tucson, pp. 89–101.

Jedicke, R., Larsen, J., Spahr, T., 2002. Observational selection effects in asteroid surveys and estimates of asteroid population sizes. In: Bottke Jr., W.F., Cellino, A., Paolicchi, P., Benzel, R.P. (Eds.), Asteroids II. Univ. of Arizona Press, Tucson, pp. 71–87.

Kargel, J.S., 2004. Mars—A Warmer, Wetter Planet. Springer/Praxis Publishing. p. 550.

Keszthelyi, L., Burr, D.M., McEwen, A.S., 2004a. Geomorphologic/thermophysical mapping of the Athabasca region, Mars, using THEMIS infrared imaging. Lunar Planet. Sci. XXXV. Abstract 1657.

Keszthelyi, L., McEwen, A., Thordarson, Th., 2000. Terrestrial analogs and thermal models for Martian flood lavas. J. Geophys. Res. 105, 15,027–15,049.

Keszthelyi, L., Thordarson, Th., McEwen, A., Haack, H., Guilbaud, M., Self, S., 2004b. Icelandic analogs to martian flood lavas. Geochemistry, Geophysics, Geosystems, vol. 5, 32 pp.

Kieffer, H.H., Zent, A.P., 1992. Quasi-periodic climate change. In: Kieffer, H.H., Jakosky, B.M., Snyder, C.W., Matthews, M.S. (Eds.), Mars. Univ. of Arizona Press, Tucson, pp. 1180–1220.

Kirk, R.L., Howington-Kraus, E., Redding, B., Galuszka, D., Hare, T.M., Archinal, B.A., Soderblom, L.A., Barrett, J.M., 2003. High-resolution topomapping of candidate MER landing sites with Mars orbital camera narrow-angle images. J. Geophys. Res. 108 (E12), 8088, 10.1029/2003JE002131.

Klingelhofer, G., 18 colleagues, 2004. Jarosite and hematite at Meridiani Planum from Opportunity's Mossbauer Spectrometer. Science 306, 1740–1745.

Lanagan, P.D., McEwen, A.S., Keszthelyi, L.P., Thordarson, Th., 2001. Rootless cones on Mars indicating the presence of shallow equatorial ground ice in recent times. Geophys. Res. Lett. 28, 2365–2367.

Lanagan, P., McEwen, A., 2003. Geomorphic analysis of the Cerberus Plains: Constraints on the emplacement of the youngest lava flows on Mars. Icarus. Submitted for publication.

Malin, M.C., Edgett, K.S., 2000a. Evidence for recent groundwater seepage and surface runoff on Mars. Science 288, 2330–2335.

Malin, M.C., Edgett, K.S., 2000b. Sedimentary rocks of early Mars. Science 290, 1927–1937.

Malin, M.C., Edgett, K.S., 2001. Mars Global Surveyor Mars Orbiter Camera: Interplanetary cruise through primary mission. J. Geophys. Res. 106, 23,429–23,570.

Malin, M.C., Caplinger, M.A., Davis, S.D., 2001. Observational evidence for an active reservoir of solid carbon dioxide on Mars. Science 294, 2146–2148.

Malin, M.C., Edgett, K.S., 2003. Evidence for persistent flow and aqueous sedimentary rocks on early Mars. Science 302, 1931–1934.

Mangold, N., 2003. Geomorphic analysis of lobate debris aprons on Mars at Mars Orbiter Camera scale: Evidence for ice sublimation initiated by fractures. J. Geophys. Res. 108, 10.1029/2002JE001885, pp. GDS 2-1.

Marquez, A., Fernandez, C., Anguita, F., Farelo, A., Anguita, J., de la Casa, M.-A., 2004. New evidence for a volcanically, tectonically, and climatically active Mars. Icarus 172, 573–581.

McEwen, A.S., Gaddis, L.R., Neukum, G., Hoffmann, H., Pieters, C., Head, J.W., 1993. Galileo observations of post-Imbrium lunar craters during the first Earth–Moon flyby. J. Geophys. Res. 98, 17,207–17,234.

McEwen, A., Keszthelyi, L., Milazzo, M., Burr, D., Christensen, P., Rice, J., Malin, M., The Themis Team, 2002. Athabasca Valles Region: New Insights from THEMIS. American Geophysical Union, Fall Meeting 2002, P11B-09.

McEwen, A.S., Turtle, E.P., Burr, D., Milazzo, M., Lanagan, P., Christensen, P., Boyce, J., The THEMIS Science Team, 2003. Discovery of a large rayed crater on Mars: Implications for recent volcanic and fluvial activity and the origin of martian meteorites. Lunar Planet. Sci. XXXIV. Abstract 2040.

Melosh, H.J., 1984. Impact ejection, spallation, and the origin of meteorites. Icarus 59, 234–260.
Melosh, H.J., 1989. Impact Cratering: A Geologic Process. Oxford Univ. Press, New York.
Melosh, H.J., Ryan, E.V., Asphaug, E., 1992. Dynamic fragmentation in impacts—Hydrocode simulations of laboratory impact. J. Geophys. Res. 97 (E9), 14,735–14,759.
Mikouchi, T., Miyamoto, M., McKay, G.A., 2001. Mineralogy and petrology of the Dar al Gani 476 martian meteorites: Implications for its cooling history and relationship to other shergottites. Meteorit. Planet. Sci. 36, 531–548.
Moore, H.J., Hodges, H.J., Scott, C.A., 1974. Multiringed basins—Illustrated by Orientale and associated features. In: Lunar and Planetary Science Conference V, vol. 1. Pergamon, New York, pp. 71–100.
Morbidelli, A., Bottke, W.F., Froeschle, Ch., Michel, P., 2002. Origin and evolution of near-Earth objects. In: Bottke, W.F., Cellino, A., Paolicchi, P., Binzel, R.P. (Eds.), Asteroids III. Univ. of Arizona Press, Tucson, pp. 409–422.
Morbidelli, A., Vokrouhlicky, D., 2003. The Yarkovsky-driven origin of near-Earth asteroids. Icarus 163, 120–134.
Mouginis-Mark, P.J., Boyce, J.M., Hamilton, V.E., Anderson, F.S., 2003. A very young, large, impact crater on Mars. International Mars Conference VI. Abstract 3004.
Mustard, J.F., Cooper, C.D., Rifkin, M.K., 2001. Evidence for recent climate change on Mars from the identification of youthful near-surface ground ice. Nature 412, 411–414.
Mutch, T.A., Arvidson, R.E., Guinness, E.A., Binder, A.B., Morris, E.C., 1977. The geology of the Viking Lander 2 site. J. Geophys. Res. 82, 4452–4667.
Nemtchinov, I.V., Shuvalov, V.V., Greeley, R., 2002. Impact-mobilized dust in the martian atmosphere. J. Geophys. Res. 107, 10.1029/2001JE001834, 5134.
Neukum, G., Ivanov, B.A., 1994. Crater size distributions and impact probabilities on Earth from lunar, terrestrial planet, and asteroid cratering data. In: Gehrels, T. (Ed.), Hazards due to Comets and Asteroids. Univ. of Arizona Press, Tucson, pp. 359–416.
Neukum, G., Koenig, B., 1976. Dating of individual lunar craters. In: Proc. Lunar Sci. Conf. VII, vol. 3. Pergamon, New York, pp. 2867–2881.
Neukum, G., Koenig, B., Fechtig, H., Storzer, D., 1975. Cratering in the Earth–Moon system—Consequences for age determination by crater counting. Lunar Planet. Sci. 6, 2597–2620.
Neukum, G., Ivanov, B.A., Hartmann, W.K., 2001. Cratering records in the inner Solar System in relation to the lunar reference system. Space Sci. Rev. 96, 55–86.
Neukum, G., 10 colleagues, The HRSC Co-Investigator Team, 2004. Recent and episodic volcanic and glacial activity on Mars revealed by the High Resolution Stereo Camera. Nature 432, 971–979.
Nyquist, L.E., Bogard, D.D., Shih, C.-Y., Greshake, A., Stöffler, D., Eugster, O., 2001. Ages and geologic histories of martian meteorites. Space Sci. Rev. 96, 105–164.
Oberbeck, V.R., Morrison, R.H., 1973. On the formation of lunar herringbone pattern. Lunar Planet. Sci. IV, 107–123.
O'Brian, D.P., Greenberg, R. The collisional and dynamical evolution of main-belt and NEA size distributions. Icarus. Submitted for publication.
Pierazzo, E., Vickery, A.M., Melosh, H.J., 1997. A reevaluation of impact melt production. Icarus 127, 408–422.
Pierce, T.L., Crown, D.A., 2002. Morphologic and topographic analyses of debris aprons in the eastern Hellas region, Mars. Icarus 163, 46–65.
Pike, R.J., 1977. Size-dependence in the shape of fresh impact craters on the Moon. In: Roddy, D.J., Merrill, R.B. (Eds.), Impact and Explosion Cratering. Pergamon, New York, pp. 489–509.
Pike, R.J., Wilhelms, D.E., 1978. Secondary-impact craters on the Moon: Topographic form and geologic process. Lunar Planet. Sci. IX, 907–909.
Plescia, J.B., 1990. Recent flood lavas in the Elysium region of Mars. Icarus 88, 465.
Plescia, J.B., 2003. Cerberus Fossae, Elysium, Mars: A source for lava and water. Icarus 164, 79–95.
Preblich, B., McEwen, A., Studer, D., 2005. Mapping rays and secondary craters from Zunil, Mars. Lunar Planet. Sci. XXXVI. Abstract 2112.
Quantin, C., Allemand, P., Mangold, N., Delacourt, C., 2004. Ages of Valles Marineris (Mars) landslides and implications for canyon history. Icarus 172, 555–572.
Rabinowitz, D., Helin, E., Lawrence, K., Pravdo, S., 2000. A reduced estimate of the number of kilometer-sized near-Earth asteroids. Nature 403, 165–166.
Reiss, D., van Gasselt, S., Neukum, G., Jaumann, R., 2004. Absolute dune ages and implications for the time of formation of gullies in Nirgal Vallis, Mars. J. Geophys. Res. 109, 10.1029.
Ruff, S.W., Christensen, P.R., 2002. Bright and dark regions of Mars: Particle sizes and mineralogical characteristics based on Thermal Emission Spectrometer data. J. Geophys. Res. 107, 10.1029/2001JE001580, 5127.
Ruff, S.W., 10 colleagues, 2001. Mars' "White Rock" feature lacks evidence of an aqueous origin: Results from Mars Global Surveyor. J. Geophys. Res. 106, 23,921–23,928.
Schaller, E.L., Murray, B.C., Byrne, S., 2003. McMurdo crater: A unique impact event on the South Polar layered deposits. Sixth International Conference on Mars. Abstract 3165.
Schmidt, R.M., Housen, K.R., 1987. Some recent advances in the scaling of impact and explosion cratering. Int. J. Impact Eng. 5, 543–560.
Schultz, P., 2002. Uncovering Mars. Lunar Planet. Sci. XXXIII. Abstract 1790.
Schultz, P.H., Gault, D.E., 1979. Atmospheric effects on martian ejecta emplacement. J. Geophys. Res. 84, 7669–7687.
Schultz, P.H., Gault, D.E., 1985. Clustered impacts—Experiments and implications. J. Geophys. Res. 90, 3701–3732.
Schultz, P.H., Lutz, A.B., 1988. Polar wanderings of Mars. Icarus 73, 91–141.
Schultz, P.H., Singer, J., 1980. A comparison of secondary craters on the Moon, Mercury, and Mars. Lunar Planet. Sci. XI, 2243–2259.
Shoemaker, E.M., 1962. Interpretation of lunar craters. In: Kopal, Z. (Ed.), Physics and Astronomy of the Moon. Academic Press, New York, pp. 283–359.
Shoemaker, E.M., 1965. Preliminary analysis of the fine structure of the lunar surface in Mare Cognitum. In: Hess, W.N., Menzel, D.H., O'Keefe, J.A. (Eds.), The Nature of the Lunar Surface. Johns Hopkins Press, Baltimore. 1966, vol. 2, pp. 23–77, JPL Tech. Report No. 32-700.
Shuvalov, V.V., 1999. Multidimensional hydrodynamic code SOVA for interfacial flows: Application to the thermal layer effect. Shock Waves 9, 381–390.
Shuvalov, V.V., 2002. Displacement of target material due to impact. Lunar Planet. Sci. XXXIII. Abstract 1259.
Siebert, N.M., Kargel, J.S., 2001. Small-scale martian polygonal terrain: Implications for liquid surface water. Geophys. Res. Lett. 28, 899–902.
Smith, P.H., 25 colleagues, 1997. Results from the Mars Pathfinder camera. Science 278, 1758–1765.
Soderblom, L.A., Condit, C.D., West, R.A., Herman, B.M., Kreidler, T.J., 1974. Martian planetwide crater distributions: Implications for geologic history and surface processes. Icarus 22, 239–263.
Squyres, S.W., 18 colleagues, 2004. In-situ evidence for an ancient aqueous environment on Mars. Science 306, 1709–1714.
Strom, R.G., Croft, S., Barlow, N., 1992. The martian impact cratering record. In: Kieffer, H., Jakosky, B., Snyder, C.W., Matthews, M.S. (Eds.), Mars. Univ. of Arizona Press, Tucson, pp. 383–423.
Stewart, S.T., O'Keefe, J.D., Ahrens, T.A., 2001. The relationship between rampart crater morphologies and the amount of subsurface ice. Lunar Planet. Sci. XXXII. Abstract 2092.
Tanaka, K.L., 1986. The stratigraphy of Mars. In: Proc. Lunar Plan. Sci. Conf. XXVII, J. Geophys. Res. Suppl. 91, E139–E158.
Teterev, A.V., 1999. Cratering model of asteroid and comet impact on a planetary surface. Int. J. Impact Eng. 23, 921–932.
Thomas, P.C., Malin, M.C., Edgett, K.S., Carr, M.H., Hartmann, W.K., Ingersoll, A.P., James, P.B., Soderblom, L.A., Veverka, J., Sullivan,

R., 2000. North–south differences between the residual polar caps on Mars. Nature 404, 161–164.

Thompson, S.L., Lauson, H.S., 1972. Improvements in the Chart D Radiation-Hydrodynamic Code III: Revised analytical equation of state. Sandia Nat. Labs, Albuquerque, NM, SC-RR-61 0714, p. 119.

Tornabene, L.L., McSween, H.Y., Moersch, J.E., Piatek, J.L., Milam, K.A., Christensen, P.R., 2005. Recognition of rayed craters on Mars in THEMIS thermal infrared imagery: Implications for martian meteorite source regions. Lunar Planet. Sci. XXXVI. Abstract 1970.

Valentine, G.A., Wohletz, K.H., 1989. Numerical models of Plinian eruption columns and pyroclastic flows. J. Geophys. Res. 94, 1867–1887.

Vasavada, A.R., Milavec, T.J., Paige, D.A., 1993. Microcraters on Mars: Evidence for past climate variations. J. Geophys. Res. 98, 3469–3476.

Vickery, A.M., 1986. Size–velocity distribution of large ejecta fragments. Icarus 67, 224–236.

Vickery, A.M., 1987. Variation in ejecta size with ejection velocity. Geophys. Res. Lett. 14, 726–729.

Weibull, W., 1951. A statistical distribution function of wide applicability. J. Appl. Mech. 18, 140–147.

Werner, S.C., Harris, A.W., Neukum, G., Ivanov, B.A., 2002. The near-Earth asteroid size–frequency distribution: A snapshot of the lunar impactor size–frequency distribution. Icarus 156, 287–290.

Werner, S.C., van Gasselt, S., Neukum, G., 2003. Continual geological activity in Athabasca Valles, Mars. J. Geophys. Res. 108, 8081.

Wilhelms, D.E., Oberbeck, V.R., Aggarwal, H.R., 1978. Size–frequency distributions of primary and secondary lunar impact craters. Lunar Planet. Sci. IX, 3735–3762.

Zahnle, K.H., Schenk, P., Levison, H., Dones, L., 2003. Cratering rates in the outer Solar System. Icarus 163, 263–289.